Identification of SARM1-dependent signaling mechanism in axon destruction program

Hyeyoung Kim

The Graduate School
Yonsei University
Department of Medical Science

Identification of SARM1-dependent signaling mechanism in axon destruction program

A Dissertation Submitted
to the Department of Medical Science
and the Graduate School of Yonsei University
in partial fulfillment of the
requirements for the degree of
Doctor of Philosophy in Medical Science

Hyeyoung Kim

June 2024

This certifies that the Doctoral Dissertation of Hyeyoung Kim is approved.

Thesis Supervisor Hosung Jung

Thesis Committee Member Chul Hoon Kim

Thesis Committee Member Phil Hyu Lee

Thesis Committee Member Jung Eun Shin

Thesis Committee Member Yongcheol Cho

The Graduate School
Yonsei University
June 2024

ACKNOWLEDGEMENTS

My doctoral journey, full of ups and downs, has finally come to an end. I still vividly remember the excitement and fear I felt when I first started my PhD course. As I brought my hopes to life one by one, I found the process enjoyable, but I also struggled with the fear of whether I would be able to finish it successfully. During those challenging times, I am deeply grateful to my advisor, Professor Hosung Jung, who was always there to share in the laughter and help solve difficulties. I have always been in awe of his brilliant intellect and hold him in the highest regard. I also extend my heartfelt thanks to Professors Chul Hoon Kim, Pil Hyu Lee, Jung Eun Shin, and Yongcheol Cho for taking the time to serve on my doctoral committee despite their busy schedules. Your invaluable advice and encouragement have meant so much to me. I am also grateful to Dr. Youngsik Choi of the Brain Science Research Institute, whose assistance with my experiments enabled me to graduate. I extend my gratitude to Professor Hyun Seok Kim, who collaborated with me on a wonderful research topic and helped bring it to fruition as a published paper. Lastly, I thank Professor Kyung-Hee Chun for her constant moral support.

I have received immense support throughout my long doctoral journey, and I want to extend my gratitude to all those who helped me. First, I would like to thank my lab members who assisted with my experiments: Dr. Jane Jung, Dr. Jiyeon Ohk, Jugeon Park, Si-hyun Park, and Mrs. Harry Kim. I am always grateful to you all.

To my beloved peers: Misun Park, Eunji Lee, Yeji Lee, Jeongseon Park, Sujin Lee, and Jieun Choi, thank you for always supporting me.

Sharing in the laughter and crying with me, the 17 years we've spent together have been wonderful. I hope we continue to be happy and maintain our friendship in the future. To Misun Park and Minhee Park, who have been like sisters to me, thank you. I truly love you both. Without you, I wouldn't be who I am today. My gratitude also extends to Professor Seok-Jun Kim, Dr. Seungwon Choi, Dr. Jung-Hwan Baek, Dr. Hyeok-Gu Kang, Hyunwoo Lee, Sunhyuk La, Yeseal Yim, Seyeon Jung, and Hyunji Han. The strong bonds we formed during our master's studies have remained because of our mutual care and support. I look forward to continuing this journey together.

To the men I love the most, thank you. My lovely husband, Junkyu Lee, you lifted me up during my toughest moments, took care of me, and loved me while I was busy with my studies. I am so grateful that you are my husband. To my handsome son, San Lee, I want to tell you that meeting you was a miracle and a blessing for me. Thank you for giving me the gift of being a mother, and I hope you continue to grow up healthy and mischievous just like you are now. And our forever kittens, Ilho and Samho, who have become senior cats, stay healthy and be together for a long time. I love you all.

To my parents-in-law, who might have felt burdened by having a daughter-in-law who was studying but silently supported me, thank you. And to my sister-in-law, Song-yi Lee, who has always been like a friend, readily helping with any difficult requests, thank you as well.

Lastly, to my beloved family, I express my gratitude to my dependable father, Soobok Kim, and my lifelong haven, my mother, Soonbok Kim. You must have had many worries as I started my PhD at a late age, but now, as I complete my doctoral journey and become a good

scientist and a mother, I am sure your pride knows no bounds. I hope you find happiness watching your grandson, San Lee, as he grows. Also, to my only brother, Heejun Kim, let's only walk only on the path of happiness from now on. Though we may not express it verbally, I support my brother's life, believing in the unspoken peace between us.

I owe my current position to the help of many people. I will continue to strive to be a passionate and diligent scientist in the future. Thank you.

TABLE OF CONTENTS

LIST OF FIGURES

LIST OF TABLES

ABSTRACT

Identification of SARM1-dependent signaling mechanism in axon destruction program

In 1850, August Waller described the stereotypical disintegration of a distal axonal fragment separated from its cell body, which is termed Wallerian degeneration. It has only recently been established that Wallerian degeneration and disease-associated degeneration of non-severed axons, particularly dying-back axon degeneration, share the molecular mechanisms and effectors, a key molecule being SARM1. Genetic deletion of the *SARM1* gene delays Wallerian degeneration, and hence current efforts are focused on whether its suppression is therapeutic in injury-induced axon degeneration, such as in chemotherapy-induced peripheral neuropathy, and disease-associated dying-back axon degeneration, such as in Parkinson's disease and amyotrophic lateral sclerosis (ALS). Originally described as a Toll-like receptor adapter protein, it was recently shown that the TIR domain of SARM1 has an unexpected nicotinamide adenine dinucleotide (NAD) hydrolase (NADase) activity, which is activated by dimerization and catalyzes the hydrolysis of NAD^+ into nicotinamide and adenine diphosphate ribose (ADP-ribose, or ADPR) or cyclic ADPR (cADPR), making it a druggable target. Developing small molecule inhibitors of SARM1 NADase activity is an active area of research. A puzzling finding is that SARM1 proteins are present in healthy axons of all ages, ready to execute the axon destruction program when triggered by axonal injury or disease-causing intracellular stimuli. Because SARM1 activation initiates an irreversible cascade of reactions to axon degeneration, this means that SARM1 is not activated at all in most axons during the lifetime. How the activation of SARM1 is tightly controlled in normal axons is largely unknown. The aim of this thesis was to elucidate the molecular mechanisms underlying the autoinhibition and activation of SARM1 in normal and diseased axons. To achieve this, I employed the APEX2 proximity biotinylation assay to selectively isolate proteins that associate with SARM1 in healthy and injured axons. Using this technique followed by affinity purification and mass spectrometry, I identified approximately 1000 proteins that are in close proximity to SARM1 proteins in axons as well as changes in their abundance in response to axonal injury. From this dataset, I drew two main

conclusions. First, I found evidence that the subcellular localization of SARM1 proteins changes in response to injury. Gene Set Enrichment Analysis (GSEA) revealed that the interactions between SARM1 and mitochondrial proteins decrease in response to injury. In contrast, the interactions between SARM1 and mediators of cellular stress responses and actomyosin increased in injured axons. These results suggest that inactive SARM1 proteins may be docked in mitochondria and redistributed using the actomyosin motor. Second, I found evidence that interactions between SARM1 and Nicotinamide phosphoribosyltransferase (NAMPT) may facilitate SARM1 activation. NAMPT converts nicotinamide to nicotinamide mononucleotide (NMN), which is known to increase SARM1 activity. I found a slight increase in interactions between SARM1 and NAMPT in injured axons, suggesting an interesting mechanism of positive feedback in SARM1 activation. In line with this idea, a newly developed small molecule inhibitor of NAMPT delayed Wallerian degeneration as well as chemotherapy-induced peripheral neuropathy. In summary, I identified proteins whose association with SARM1 proteins changes in response to axonal injury as intended and made two new findings relevant to understanding the molecular mechanisms underlying SARM1 activation and its prevention. The new dataset and findings made in this thesis will contribute to a deeper understanding of SARM1 activation in diseased and injured axons and may shed light on therapeutic strategies to prevent SARM1 activation and SARM1-dependent axon degeneration and neurodegenerative diseases.

Key words: SARM1, axon destruction, wallerian degeneration, neuropathy

1. Introduction

Axons are essential for the functioning of the nervous system, and their destruction precedes many neurodegenerative diseases. Research on axonal degeneration has been very active in recent years. Over a century after Wallerian degeneration-induced axonal degeneration was first described, its relationship with neurodegenerative diseases has emerged: most, if not all, neurodegenerative diseases may start with the degeneration of axon terminals before any evidence of cell death. This has led to the hypothesis that blocking axon degeneration may delay or prevent the progression of neurodegeneration. A surprising finding was that Wallerian degeneration requires gene function, indicating that axon degeneration is an active destruction program of a subcellular compartment [1-4].

Axonal damage impedes the axonal transport of vital molecules like nicotinamide mononucleotide adenylyl transferase 2 (NMNAT2) from the soma. Consequently, NMNAT2, characterized by a short half-life, undergoes rapid degradation in the distal axon, triggering SARM1-dependent degeneration. Injury-induced calcium influx may instigate the destructive program, necessitating *SARM1* gene functionality. Conversely, nicotinamide mononucleotide adenylyltransferase 2 (*Nmnat2)* gene gain-of-function, exemplified by the expression of *slow Wallerian degeneration (Wlds)*, a cytosolically mislocalized mutant form of NMNAT2, retards Wallerian degeneration (Figure 1) [5].

In particular, the primary focus to mitigate damage to the nervous system is being focused to *SARM1*, the knockout of which prevents Wallerian degeneration. SARM1 is a Toll-like receptor adapter protein required for the normal and rapid rate of Wallerian degeneration. It was recently discovered that SARM1 is a crucial factor for Wallerian degeneration in mice and fruit flies [6, 7]. During axonal degeneration, SARM1 serves as the initiator of axon degeneration in response to various forms of damage stimulation. SARM1 consists of three distinct domains: the armadillo-like repeats (ARM) domain involved in auto-inhibition, the sterile alpha motifs (SAMs) domain involved in multimerization, and the Toll/interleukin-1 receptor (TIR) domain responsible for NADase activity (Figure 2A). A significant finding was that the dimerized SARM1-TIR domain exhibits unexpected NADase activity that

hydrolyzes NAD^+ into nicotinamide and ADP-ribose (ADPR) or cyclic ADPR (cADPR) [8]. The intrinsic NADase activity of the SARM1-TIR domain was demonstrated through cell-free transcription and translation TIR protein experiments [9]. Importantly, the rapid depletion of NAD^+ is adequate to trigger axonal degeneration. Together with the Wallerian degeneration-delaying effect of NMNAT2, an enzyme that produces NAD^+, this suggests axon degeneration is closely linked to local regulation of NAD^+ metabolism [8]. However, the detailed mechanism by which axon degeneration is regulated by SARM1, NMNAT2 and NAD^+ remains unclear. The discovery of the enzyme activity of SARM1 presents a clear direction in preventing axon degeneration, and small molecule inhibitors for SARM1 are actively being developed worldwide [10].

Recently, the first crystal structure of SARM1 was solved, which consists of a homo-octamer bridged by SAMs. The ARM domain appears to inhibit the NADase activity of the TIR domain, possibly by binding to NAD^+ and protecting it from the TIR domain (Figure 2B) [5, 11]. It is unclear whether NAD^+ loss is the cause of axon degeneration even after SARM1 is activated. If it is a loss of NAD^+, this is because the level must be very low to be effective. NAD^+ is reduced by 50% in the sciatic nerve dissected from *Sarm1* knockout mice and by 80% in DRGs amputated in *Sarm1* knockout mice within 5 days of injury. However, in both cases, the axon survives for a long period. Interestingly, the protein Axundead (*Axed*) in *D. melanogaster* was found to act downstream of dSarm, a protein required for rapid Wallerian degeneration [7]. Axed has the potential to act as an executor of degeneration. Axed is a BTB/BACK-containing protein with no apparent role in calcium or NAD^+ metabolism, but its ability to protect in the presence of activated dSarm or in the absence of dNmnat implies that it affects NAD^+ in some way. Like the Axed protein, it could be suggested that there are more proteins that can change in a SARM1-dependent manner. The above two pieces of evidence suggest that not only NAD^+ but also other factors play a role in the delay of SARM1-dependent Wallerian degeneration. Although these studies showed a glimpse of SARM1 activation and inhibition, much remains unanswered. For example, it is unknown how SARM1 is kept inactive in healthy axons and which various axonal damages, such as physical, chemical, biological insults, commonly activate SARM1. Moreover, it is not known which molecules destroy the axon once SARM1 is activated.

Therefore, I aimed to investigate which molecules are involved in the SARM1-dependent axonal destruction program. My objective was to induce SARM1 activation and subsequently identify the proximity proteins of SARM1 present within the axons. By characterizing proteins that bind to both inactive and active SARM1, I sought to uncover the molecular switch that regulates SARM1 activation (Figure 3).

To prove this, the identification of all proteins directly or indirectly associated with inactive and active SARM1 is necessary. Therefore, the APEX2 proximity biotinylation system is considered an appropriate experimental tool.

APEX2 is a monomeric peroxidase that can be expressed in cells in the form of a fusion protein with the protein of interest. Upon treatment with a biotin-phenol ligand, APEX2 converts phenol into a radical in the presence of H_2O_2. The radical persists for approximately 1 ms and can either return to its original state or recombine. Through diffusion, it can spread up to a maximum distance of about 20 , thereby biotinylating only adjacent proteins. Following biotinylation, proteins can be isolated using biotinylation affinity purification, and their identities can be determined through mass spectrometry analysis (Figure 4) [12-14].

My goal is to induce the activation and deactivation of SARM1 in axons using the APEX2 proximity biotinylation system, followed by affinity purification of proteins directly or indirectly associated with SARM1 and their identification through mass spectrometry analysis (Figure 5). By conducting these experiments in both activated and inactivated states of SARM1 within axons, potential inhibitors and facilitators can be identified, suggesting new candidates for SARM1 activity regulation, and ultimately proposing novel strategies for preventing neurodegeneration caused by injury or disease.

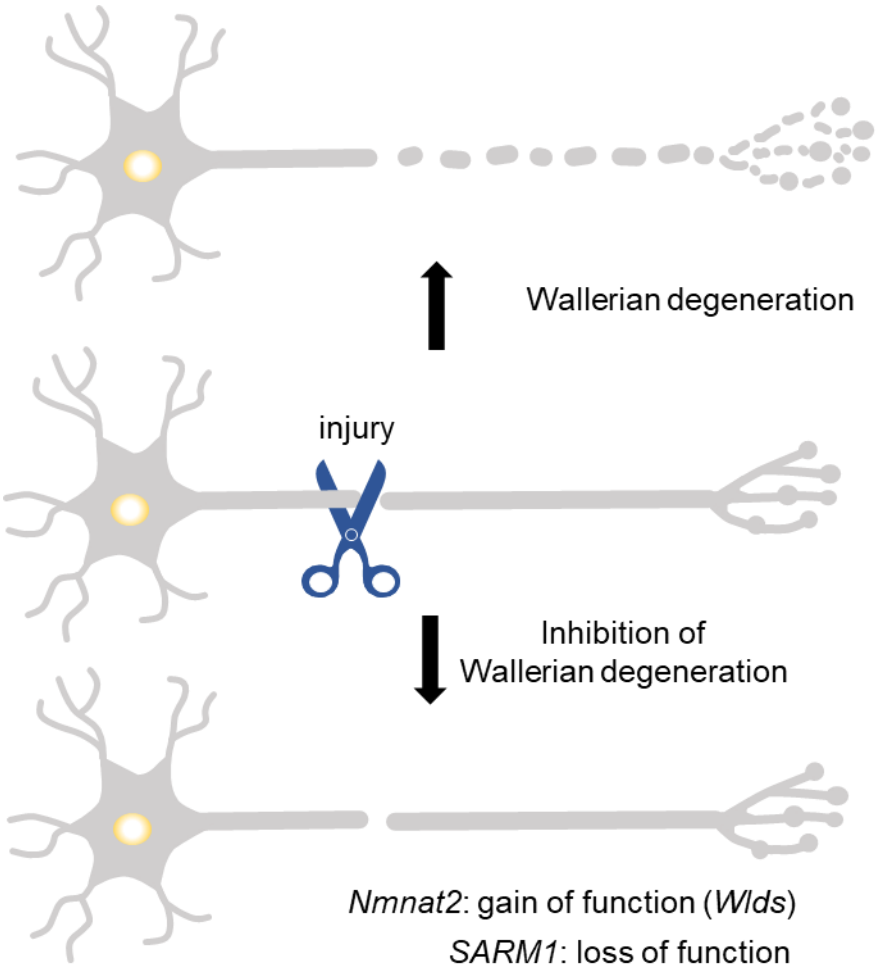

Figure 1. Molecular pathways mediating Wallerian degeneration (WD). Wallerian degeneration induced by injury is delayed by the introduction of the *Wlds* gene and the knockout of the *SARM1* gene.

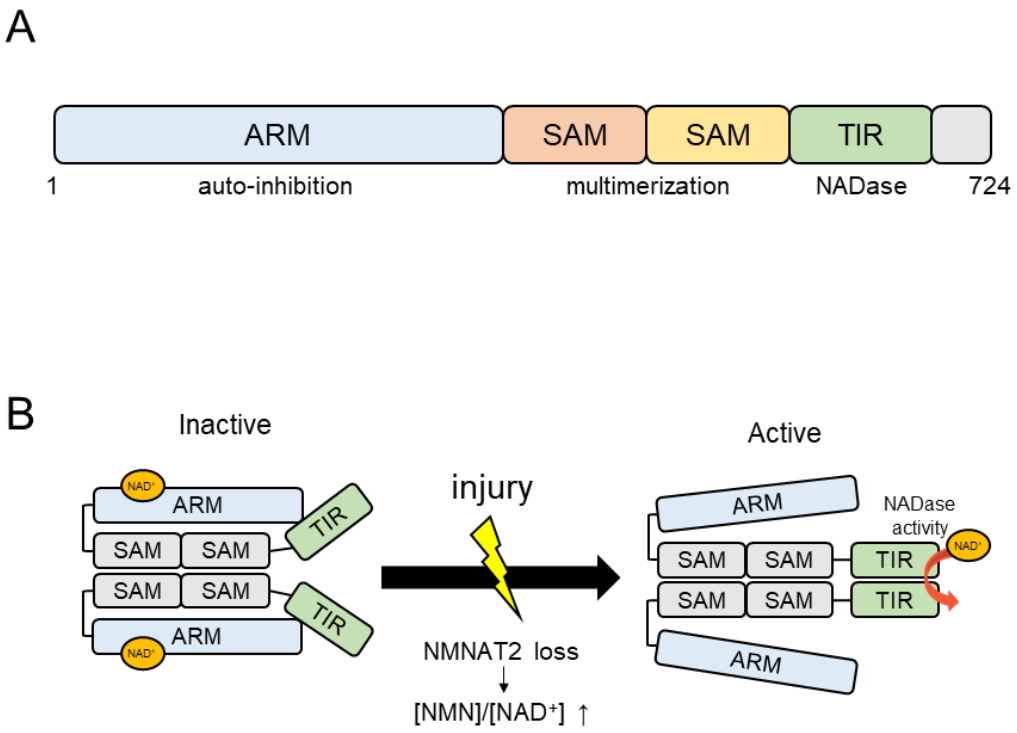

Figure 2. SARM1 structure and function. (A) SARM1 (sterile alpha and TIR motif-containing protein 1) consists of an auto-inhibitory armadillo domain (ARM), two tandem sterile alpha motif (SAM) domains, and a toll/interleukin-1 receptor (TIR) domain. (B) The ARM domain interacts with the TIR domain to prevent the activation of SARM1. The schematic diagram of SARM1 after damage-induced activation shows self-inhibition of ARM-TIR multimerization, leading to the enzymatic degradation of NAD^+ [5].

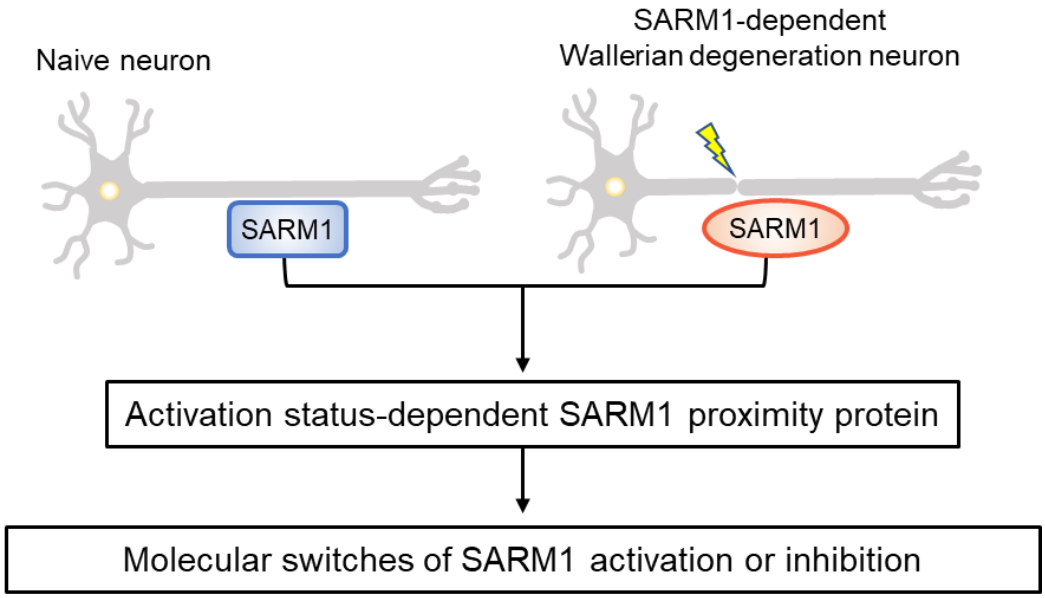

Figure 3. Identification of proteins associated with axonal destruction program execution, modulated by SARM1 during Wallerian degeneration, through proteomic analysis.

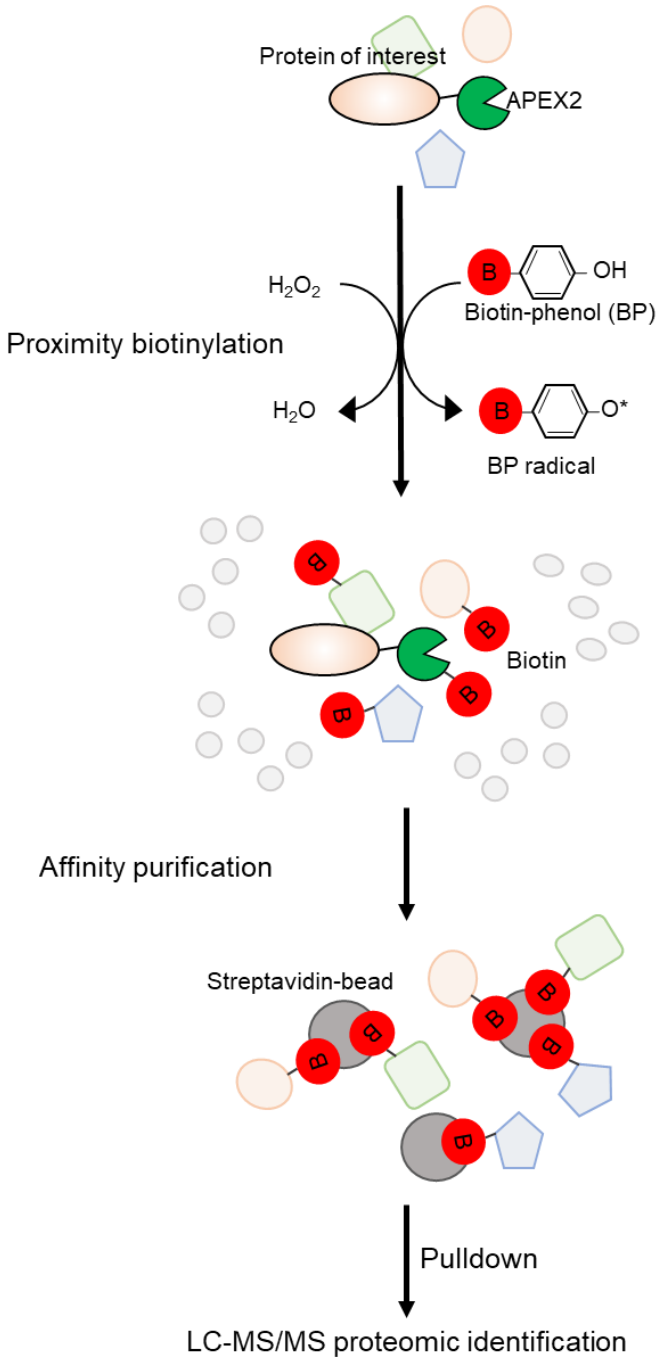

(Continued)

Figure 4. Scheme showing APEX2-catalyzed biotinylation. Live cells are incubated with a biotin-phenol probe for 30 minutes and then treated with 1 mM H_2O_2 for 1 minute to initiate biotinylation. APEX2 covalently tags proximal endogenous proteins by catalyzing the one-electron oxidation of biotin-phenol to form a biotin-phenoxyl radical. The biotinylated proteins can be identified through mass spectrometry analysis after affinity purification.

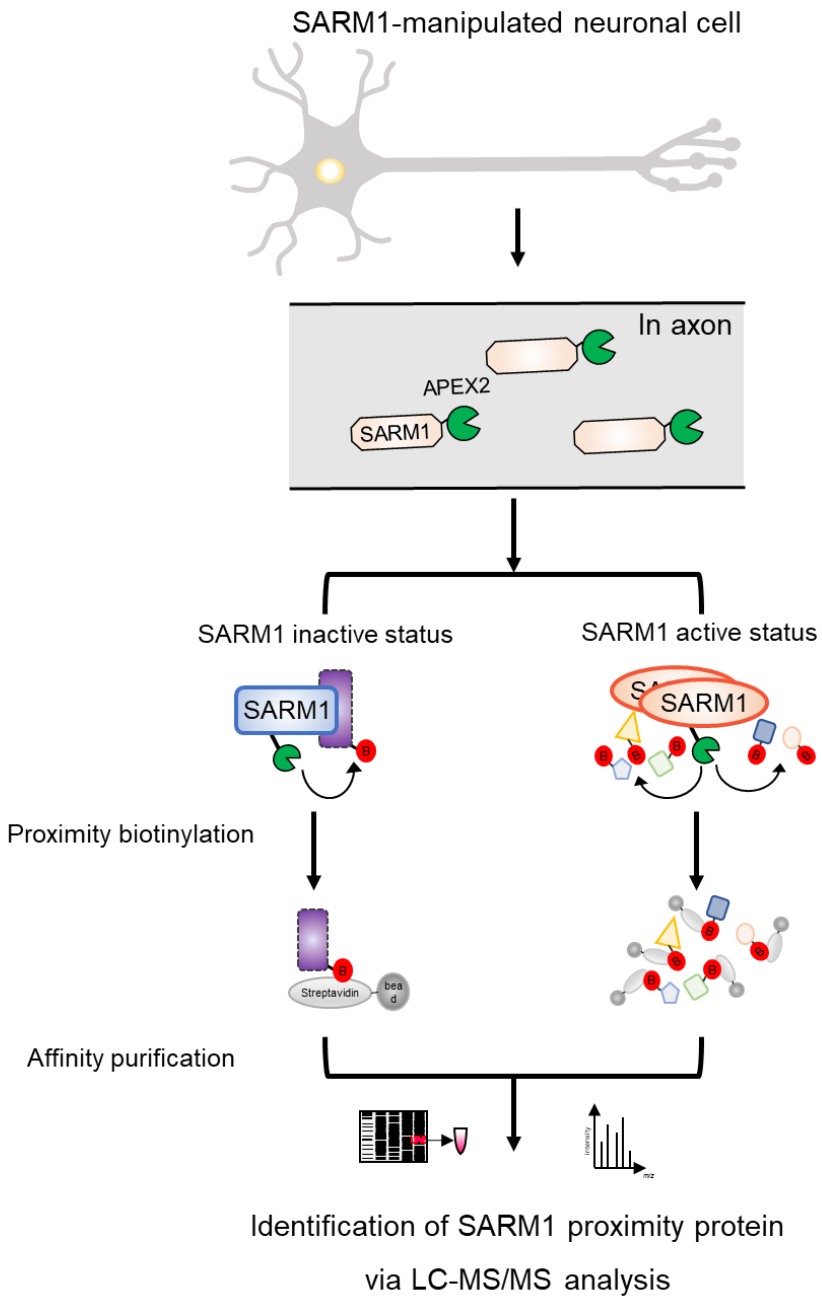

Figure 5. Experimental scheme for derivation of SARM1-dependent facilitator or inhibitor protein via APEX-catalyzed biotinylation.

2. Materials and Methods

2.1. Cell culture and mouse

HEK293T (human embryonic kidney cell line) and SH-SY5Y (human neuroblastoma cell line) were cultured in Dulbecco's Modified Eagle's Medium (DMEM, Gibco, USA) supplemented with 10% fetal bovine serum (FBS, Sigma, USA) and 1% antibiotic-antimycotic solution (Invitrogen, USA) at 37°C in a humidified atmosphere containing 5% CO_2. When the cells reached 90% confluence, they were sub-cultured using Trypsin-EDTA (Sigma, USA). Wild-type mice were obtained from KOATECH (Korean Animal Technology, Korea), and all animal procedures were conducted following the guidelines of the Laboratory Animals of Yonsei University School of Medicine.

2.2. Plasmid

2.2.1. *SARM1* sgRNA

To generate a SARM1 knockout SH-SY5Y cell line, a single guide RNA (sgRNA) targeting exon 8 of SARM1 (5′- ATTGTGACTGCTTTAAGCTG -3′) was inserted into the pL-CRISP R.EFS.GFP vector (#57818, Addgene, USA). Targeting exon 8 was chosen due to its proximity to the putative enzymatic site (E642) [15].

2.2.2. SARM1-APEX2 fusion protein

The coding DNA sequence (CDS) of the SARM1 gene was synthesized based on the reference sequence in GenBank (NM_015077.3). The SARM1 protein was then inserted into the pcDNA3-APEX2-NES vector (#49686, Addgene). APEX2 fusion constructs were subsequently transferred to the Lentiviral vector pLECE-GFP. The cloning primers used were: 5’- GGATCCATGGTCCT GACGCT-3’ and 5’- GCGGCCGCCTATTAGTCCAG-3’.

2.3. Lentivirus particle construction

To establish cell lines expressing the SARM1-APEX2 fusion protein stably, lentiviral particles were generated by transfecting HEK-293T cells with the corresponding lentiviral

vectors, along with pMD2.G (#12259, Addgene, USA) and psPAX2 (#12260, Addgene, USA). After 3 days, the transfected cells were centrifuged to collect the supernatant. The supernatant was then filtered (16555K, Sartorius, Germany) and either used immediately to infect the target cell line or stored at 4°C for up to 1 week or at -80°C for longer-term storage.

2.4. Western blot

Cell lysates were prepared by lysing cells in RIPA buffer (1% NP-40; 0.1% sodium dodecyl sulfate; 0.5% deoxycholate; 150 mM NaCl; 50 mM Tris, pH 7.5) supplemented with a protease inhibitor cocktail (Sigma, USA), Phosphatase inhibitor cocktail 2 (Sigma, USA), and Phosphatase inhibitor cocktail 3 (Sigma, USA). Protein quantification was performed using the Pierce BCA protein assay kit (Thermo, USA). Twenty micrograms of total protein from each lysate were separated by SDS-PAGE gels and transferred onto PVDF membranes. The membranes were then blocked in 5% skim milk in 0.05% Tween-20 with 1X TBS (TBST). Primary antibodies were diluted 1:1000 in 5% BSA or 5% skim milk in TBST buffer and incubated with the blots for 1 hour at room temperature or overnight at 4°C. HRP-conjugated secondary antibodies (anti-mouse or anti-rabbit) were diluted 1:5000 in 5% skim milk in TBST buffer and incubated with the membranes for 1 hour at room temperature. The antibodies used in this study included anti-SARM1 (#13022) from Cell Signaling Technology, mouse anti-Actin (sc-47778) from Santa Cruz Biotechnology, and mouse anti-Flag (F1804) from Sigma-Aldrich. HRP-conjugated secondary antibodies (rabbit anti-mouse [ab6728] and goat anti-rabbit [ab6721]) were purchased from Abcam. Membranes were then incubated with primary and secondary antibodies, and antibody binding was detected using Pierce ECL Plus Western Blotting Substrate (32134, Thermo, USA) and visualized with a LAS-4000 (Fujifilm) detector following the manufacturer's instructions.

2.5. Stable cell line construction

2.5.1. SARM1 knockout cell line

SH-SY5Ycells were transfected with the *SARM1* sgRNA vector and cells expressing GFP were sorted by Fluorescence-Activated Cell Sorting (FACs). Seed single cells into 96 well plates and single-cell colonies were validated by genomic DNA sequencing and

protein expression using western blot. Sequencing primer: 5′-TATTACACTACAAGG GTTAAGG T-3′ and 5′-TTCAGAAAGGA CGATGG AAATG-3′

2.5.2. SARM1-APEX2 fusion protein stable cell line

SH-SY5Y *SARM1* knockout cells were infected with SARM1-APEX2 fusion protein lentivirus particles and cells expressing GFP were sorted by Fluorescence-Activated Cell Sorting (FACs). Cells sorted by GFP were validated by protein expression using western blot.

2.6. SH-SY5Y cell differentiation

To optimize the matrix for differentiation, culture plates were coated with ECM diluted 1:100 in DMEM (E0282, Sigma) for 1 hour at 37°C in a humidified 5% CO_2 atmosphere and then dried. Differentiated cells were cultured using three different media. SH-SY5Y cells were plated on 10 μg/ml laminin and incubated in complete DMEM (Day 0) and changed to DMEM containing 2.5% FBS and 10 μM all-trans retinoic acid (RA) for 1 week (Day 7) to induce differentiation. On day 8 of differentiation, DMEM containing 1% FBS and 10 μM all-trans retinoic acid (RA, R2625, Sigma) was added. By day 10 of differentiation, cells were split in 1:1 onto ECM-coated culture plates and after 1 day, changed to differentiation media 3 (Neurobasal media: #12349-015, Gibco; 1X B-27: #17504044 Gibco; 1X N2 supplement: 17502048, Gibco; 20 mM KCL: Invitrogen, AM9640G; 1X antibiotic antimycotic: Invitrogen, 15240062; 2 mM Glutamax: 35050061, Gibco; 50 ng/ml BDNF: 450-02, Pepprotech; 2 mM db-cAMP: D0627, Sigma; Retinoic acid: R2625, Sigma). Finally, on day 18 of differentiation, cells were ready for experiments. The differentiation medium was replenished after 48 hours. A compartmental chamber (PET track-etched membrane 6-well format Cell culture insert with a pore size of 1 μm, 353102, Flacon) was used during injury experiments [16, 17].

2.7. Immunocytochemistry (ICC)

The cells were fixed using 4% paraformaldehyde and then permeabilized with 0.1% Triton-X 100 in PBS for 10 minutes at room temperature. Subsequently, they were treated

with 10% BSA in PBST (PBS with 1% Tween 20) for 1 hour at room temperature. Following this, the samples were incubated with the respective primary antibodies, followed by incubation with Alexa Fluor 488, 555, and 647-conjugated goat anti-mouse and/or rabbit IgG antibodies (Invitrogen). DAPI was used to stain the nuclei. Finally, the specimens were observed using a confocal laser scanning microscope (Zeiss-Yonsei Imaging Facility; LSM 700; Carl Zeiss, Jena, Germany).

2.8. APEX2 labeling and Streptavidin bead enrichment of biotinylated proteins

Labeling of living cells was conducted 18-24 hours after plating SH-SY5Y SARM1 knockout cells stably expressing the corresponding APEX2 fusion construct. APEX2 labeling began by replacing the medium with fresh medium containing 500 mM biotin-phenol (Sigma) and incubating at 37°C under 5% CO_2 for 30 minutes. Subsequently, H_2O_2 was added to each well to a final concentration of 1 mM, and the plate was gently agitated for 1 minute. The reaction was quenched by replacing the medium with an equal volume of 5 mM Trolox, 10 mM sodium ascorbate, and 10 mM sodium azide in Dulbecco's phosphate-buffered saline (DPBS). Cells were washed three times with DPBS containing 5 mM Trolox and 10 mM sodium ascorbate before proceeding to the experiment. Unlabeled controls underwent identical processing steps, except for the omission of the H_2O_2. APEX-labeled cell pellets served as input for each sample. The pellets were lysed in RIPA lysis buffer supplemented with 8 M urea for 10 minutes at 4°C. After centrifugation at 13,000 rpm for 10 minutes at 4°C, detergents were removed using Detergent Removal Spin Columns (Thermo, #8777). Streptavidin-coated magnetic beads were washed with RIPA buffer without detergents, and total protein cell lysate from each sample was separately incubated with 450 µl of magnetic beads with rotation for 1 hour at room temperature or overnight at 4°C. The beads were subsequently washed twice with 1 mL of RIPA lysis buffer without detergents, once with 1 mL of 1 M KCl, once with 1 mL of 0.1 M Na_2CO_3, once with 1 mL of 2 M urea in 10 mM Tris-HCl (pH 8.0), and twice with 1 mL of RIPA lysis buffer without detergents. For streptavidin blot analysis, biotinylated proteins were eluted by boiling the beads in protein loading buffer supplemented with 20 mM dithiothreitol (DTT) and 2 mM biotin, and then run on SDS-polyacrylamide gel electrophoresis (PAGE) gel [12, 14, 18, 19].

2.9. *Xenopus tropicalis* experiments

Xenopus tropicalis retinal axon labeling and degeneration imaging were conducted as previously described [20]. To summarize, stage 27-28 *Xenopus tropicalis* embryos were anesthetized, and an EGFP-encoding plasmid was introduced into the optic vesicle via targeted electroporation. By stage 41, when retinal ganglion cell axons had reached the optic tectum, the optic nerve originating from the electroporated retina was severed. Drug administration commenced at the time of axotomy and continued throughout the experimental period. Imaging of EGFP-labeled retinal axons projecting to the contralateral optic tectum was performed using a laser scanning confocal microscope (LSM700, Zeiss, Germany).

2.10. Measurement of NAD^+ concentration and NMN-to-NAD^+ ratio in *Xenopus tropicalis* embryos

2.10.1. Measurement of NAD^+ concentration

At stage 41, *Xenopus tropicalis* embryos underwent axotomy, and the compounds (control, FK866, A4276H) were applied at a concentration of 10 μM for 48 hours. NAD^+ levels were assessed using NAD/NADH-Glo Assays (Promega, G9071) and a microplate reader (EG&G Berthold, Centro XS3 LB960).

2.10.2. Measurement of NMN-to-NAD^+ concentration

The compound (control, FK866, or A4276H) was applied at a concentration of 10 μM for 48 hours. Tadpole samples were collected into three groups (WT, FK866, A4276H), with each group containing 50 mg of sample in a 1.5 ml tube (n=4). Nicotinamide mononucleotide (NMN) and nicotinamide adenine dinucleotide (NAD^+) were extracted from 500 μL of pre-cooled (-20°C) 80% methanol with the internal standard (ISTD) 2-chloroadenosine. The ISTD was added to all samples at a concentration of 40 ng/mL for quality control. Methanol and ISTD were added to the samples, followed by vortex mixing for 4 minutes and centrifugation for 10 minutes at 16,000 ×g and 4°C. Subsequently, 500 μL of chloroform was added to the supernatants, and centrifugation was performed for 10 minutes at 16,000 ×g and 4 °C. This chloroform extraction step was repeated, and the

supernatants were dried using a speed vacuum concentrator with a cold trap (CentriVap Cold Traps, Labconco, Kansas City, MO, USA). Each dried sample was reconstituted in 100 µL of HPLC-grade water and centrifuged for 10 minutes at 16,000 ×g and 4 ℃. The supernatants were transferred to vials for liquid chromatography–mass spectrometry analysis. Extracted samples were injected into an ACQUITY UPLC BEH Amide 1.6 µm C18 130Å, 100 mm × 2.1 mm column (Waters, Milford, MA, USA) and separated over 6 minutes (0.6 mL/minute) using a gradient of solvent B at 40 ℃. Solvent B consisted of 20 mM ammonium acetate in water (pH 3.2 with formic acid) and acetonitrile (100%). The injection volume was 2 µL. Polarity was set at positive mode. The liquid chromatography system was coupled to a SCIEX QTRAP 5500+ (AB SCIEX, Framingham, MA, USA) with Nexera series LC-40 (Shimadzu Corporation, Kyoto, Japan). Single reaction monitoring (SRM) analysis was performed, with optimization of decluttering potential (DP), collision energy (CE), and collision cell exit potential (CXP) for the target compound. Each target was optimized with a total of two transitions, one for quantification and the other for qualification. Liquid chromatography-mass spectrometry experiments were performed by the Prometabio Research Institute (Prometabio Co., Ltd. Hanam-si, Gyeonggi-do, Republic of Korea), and data acquisition and processing were carried out using Analyst (AB SCIEX, version 1.7.3 HotFix 1) and SCIEX OS (AB SCIEX, version 3.0.0.3339) [21].

2.11. Mass spectrometry

The cells were disrupted using a lysis buffer comprising 50 mM Tris-HCl (pH 7.5), a protease inhibitor cocktail, 1 mM phenylmethylsulfonyl fluoride (PMSF), 150 mM NaCl, 2 mM EDTA, 4% SDS, 1% Triton X-100, 1% sodium deoxycholate, and 8M urea. Prior to immunoprecipitation of biotinylated proteins, detergent removal columns were utilized. Following stringent washing steps, the precipitates were resuspended in 50 mM TEAB buffer containing protease and phosphatase inhibitors. For trypsin digestion, each 100 µL sample was treated with 2 µL of 500 mM dithiothreitol (DTT) at 56°C for 30 minutes, followed by 4 µL of 500 mM iodoacetamide for 25 minutes, and then 2 µL of 50 mM DTT. Subsequently, 1 µL (0.5 µg/µL) trypsin was added and incubated overnight at 37°C. The trypsin-digested peptides were purified using C18 tips (Thermo) and eluted in 15 µL of 0.1% formic acid for

injection into the Ultimate 3000 RSLCnano system (LC) coupled with a Q-Exactive Plus Orbitrap mass spectrometer (MS, Thermo Fisher). Chromatographic separation of peptide fractions was achieved using an Ultimate 3000 RSLCnano System equipped with a PepMap 100 C18 LC loading column and a PepMap RSLC C18 analytical column. The LC flow rate was maintained at 0.3 μL/minute for 135 minutes. Mass spectrometric analysis employed a full-scan MS approach within the 350-2000 m/z range, along with data-dependent MS/MS acquisition. Raw LC-MS/MS data were processed using Proteome Discoverer 3.0 (Thermo Fisher Scientific) via MS2 spectra searching with the Sequest algorithm against the human Uniprot database (as of September 13, 2023). A mass tolerance of 10 ppm was applied for peptide precursors, with a fragment tolerance of 0.02. False discovery rates (FDRs) for proteins and peptide spectral matches (PSMs) were limited to 1%. Data normalization was conducted based on total peptide abundance to identify proteins exhibiting differential expression. Data analysis was performed using the R environment following the protocol described in a previous publication [22]. This experimental procedure was conducted by Youngshik Choe at the Korea Brain Research Institute (KBRI).

2.12. Mouse dorsal root ganglion (DRG) cell culture

Perinatal mouse dorsal root ganglia (DRG) were aseptically harvested and subjected to enzymatic treatment with 0.25% trypsin at 37°C for 15 minutes. Subsequently, the trypsin activity was neutralized using fetal bovine serum, and the DRG were centrifuged at 3000 rpm for 5 minutes. The cells were then suspended in Neurobasal A medium supplemented with 2% B-27, 0.5% glutamine, 1% antibiotic-antimycotic, and 10 ng/mL of nerve growth factor (NGF). Following dissociation into individual cells through trituration, the cells underwent pre-plating on an uncoated Petri dish to eliminate adherent cells. The loosely attached neurons were subsequently plated into the somal compartment of a microfluidic device that had been pre-coated with poly-L-lysine and Laminin. The axonal compartment received a higher concentration of NGF (50 μM) to stimulate axon growth. Vincristine and paclitaxel were introduced into the axonal compartments to induce axonal degeneration, with prior treatment of A4276 (2 μM) and FK866 (5 μM) 24 hours before exposure to these chemotherapeutic agents. Specifically, vincristine was administered at a concentration of 40 nM for 24 hours, followed by treatment with 100 nM paclitaxel for 48 hours [21, 23].

2.13. Quantification of axon degeneration in culture

The cell cultures were fixed at designated time points using 4% paraformaldehyde in PBS. To visualize stable microtubules in the axons, immunocytochemistry was performed using an antibody targeting acetylated alpha-tubulin (Abcam, ab125356) and an Alexa Fluor 488-conjugated secondary antibody (Thermo Fisher, A-21206). Samples were immunostained and imaged under consistent settings for subsequent quantitative analyses. The axon fragmentation index, representing the proportion of lost axonal length, was determined as follows: Axonal traces in images were manually outlined as segmented lines. The acetylated alpha-tubulin channel was thresholded to create a binary image, onto which axonal traces were overlaid. Subsequently, the axon fragmentation index for the entire image was computed as the sum of the lengths of axons unstained with acetylated alpha-tubulin divided by the total sum of axonal traces. All experiments were conducted with a minimum of three independent biological replicates [21].

3. Results

3.1. Construction of tool for SARM1-dependent axon destruction proximity protein

3.1.1. Construction of *SARM1* knockout neuronal cell line

The first step is to establish a model capable of controlling SARM1 activation. Specifically, a *SARM1* knockout model was developed using the widely utilized human neuronal SH-SY5Y cell line. The SH-SY5Y cell line, derived from human neuroblastoma cells, serves as an excellent model for various neuronal developmental and disease-related studies. Its capability to differentiate into neuronal cells under specific conditions makes it particularly suitable for investigating neurological disorders. Additionally, its amenability to genetic manipulation and ability for mass culture and differentiation make it an ideal material for molecular biology research. Initially, SH-SY5Y cells were induced to differentiate to confirm successful differentiation. The cells were first induced into a pre-differentiation stage by culturing them in DMEM medium containing 2.5% FBS and 10 μM retinoic acid for one week, followed by three days in DMEM medium containing 2.5% FBS and 10 μM retinoic acid. Subsequently, differentiation was induced from the 11th day onwards by culturing them in Neurobasal medium supplemented with BDNF and N2 (Figure 6A). After inducing differentiation for a total of 18 days, the presence of axons was confirmed by staining for the neuronal cell markers Tuj1 and Tau. Expression of Tuj1 and Tau, indicative of axon induction in SH-SY5Y cells, was observed only in cells where differentiation occurred successfully (Figure 6B and 6C).

Next, the Clustered Regularly Interspaced Short Palindromic Repeats/CRISPR-associated protein 9 (CRISPR/Cas9) technology was employed to introduce a frameshift mutation into the *SARM1* gene, thereby creating a mutant cell line unable to produce functional SARM1 protein. The CRISPR/Cas9 technology is globally acknowledged as an efficient tool for genetic manipulation tool, functioning as a genetic scissor capable of

effectively deleting genes [24].

The strategy involves generating vectors expressing Cas9/sgRNA/GFP and transfecting them into parental cells to create cells that express GFP. Subsequently, single-cell sorting and clonal expansion culture via FACs (Fluorescence-Activated Cell Sorting) are conducted to identify *SARM1* knockout clones (Figure 7). Initially, a single guide (sg) RNA targeting *SARM1* exon 8 was designed. Exon 8 was selected as the target since it is near the putative enzymatic site E642, aiming to prevent the coding of functional SARM1 protein (Figure 8A). To ensure successful selection, GFP was co-expressed with sgRNA and Cas9. Visualization confirmed the expression of the sgRNA target vector in the SH-SY5Y cell line, and expression of GFP was confirmed using fluorescence microscopy. GFP-expressing cells were sorted as single cells using FACs and cultured (Figure 8B). After single-cell clones were grown in 96 wells, *SARM1* knockout was confirmed through genome sequencing and protein expression levels. Sanger sequencing (Macrogen, Seoul) confirmed frameshift mutations at the target site in the genome (Figure 9A, clone 2). Additionally, western blot analysis confirmed the absence of SARM1 protein expression in Clone 2 cells (Figure 9B).

Consequently, a *SARM1* knockout cell line was successfully established. Although Wallerian degeneration due to axonal damage is delayed in the *SARM1* deficiency model [6], the mechanism by which SARM1 promotes the axonal destruction program remains unknown. This outcome suggests the feasibility of experimentally introducing an activatable *SARM1* gene, providing a means to identify downstream pathways of SARM1 activation.

A

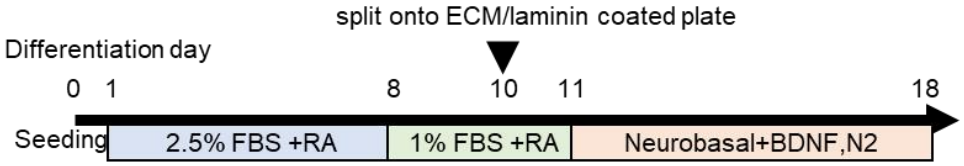

B

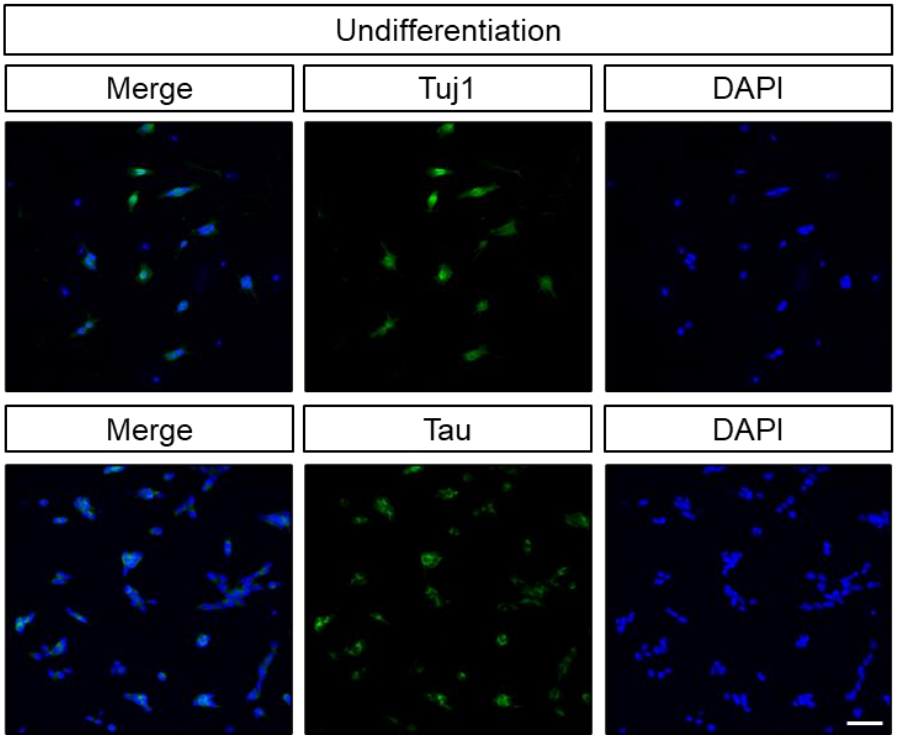

(Continued)

C

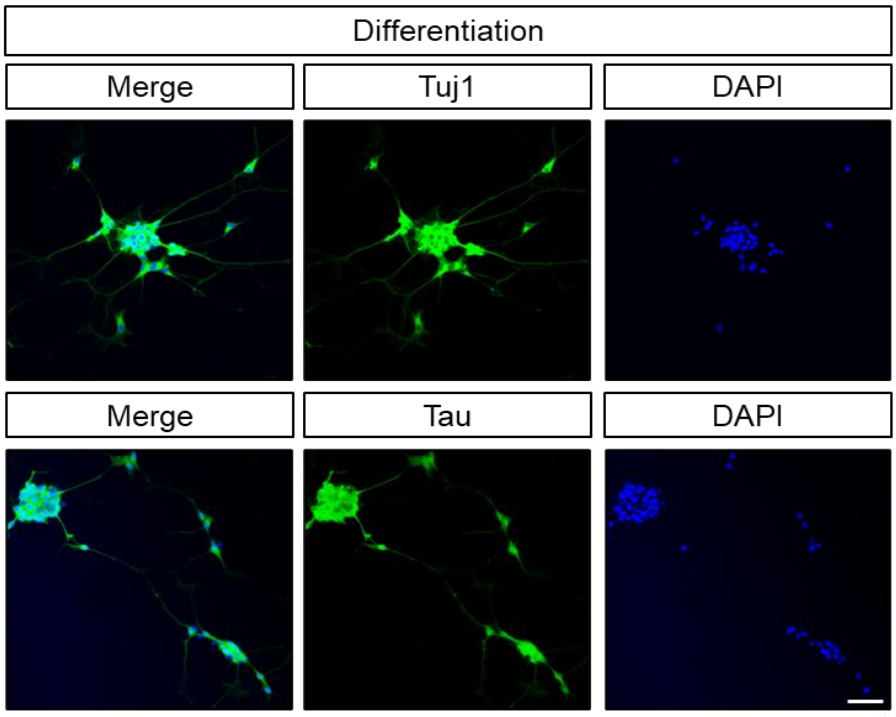

Figure 6. The differentiation process of SH-SY5Y cells and the morphology of neuronal differentiation. (A) Differentiation process of SH-SY5Y cells. (B and C) Staining of undifferentiated (B) and differentiated (C) SH-SY5Y cells with axonal markers Tuj1 and Tau. The scale bar is 50 μm.

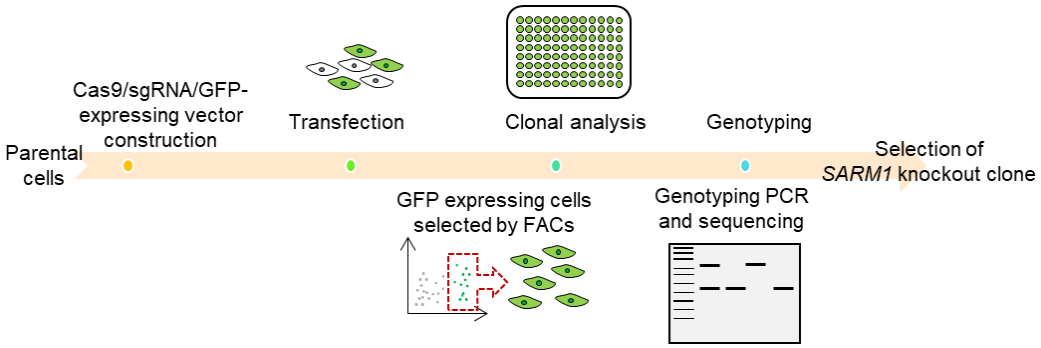

Figure 7. Workflow for CRISPR/Cas9-mediated *SARM1* knockout neuronal cell line. After transfecting parental cells with a Cas9/sgRNA/GFP expression vector, GFP-expressing cells were sorted using FACs and followed by single-cell clonal expansion. Subsequently, genotyping was performed to identify *SARM1* knockout clones.

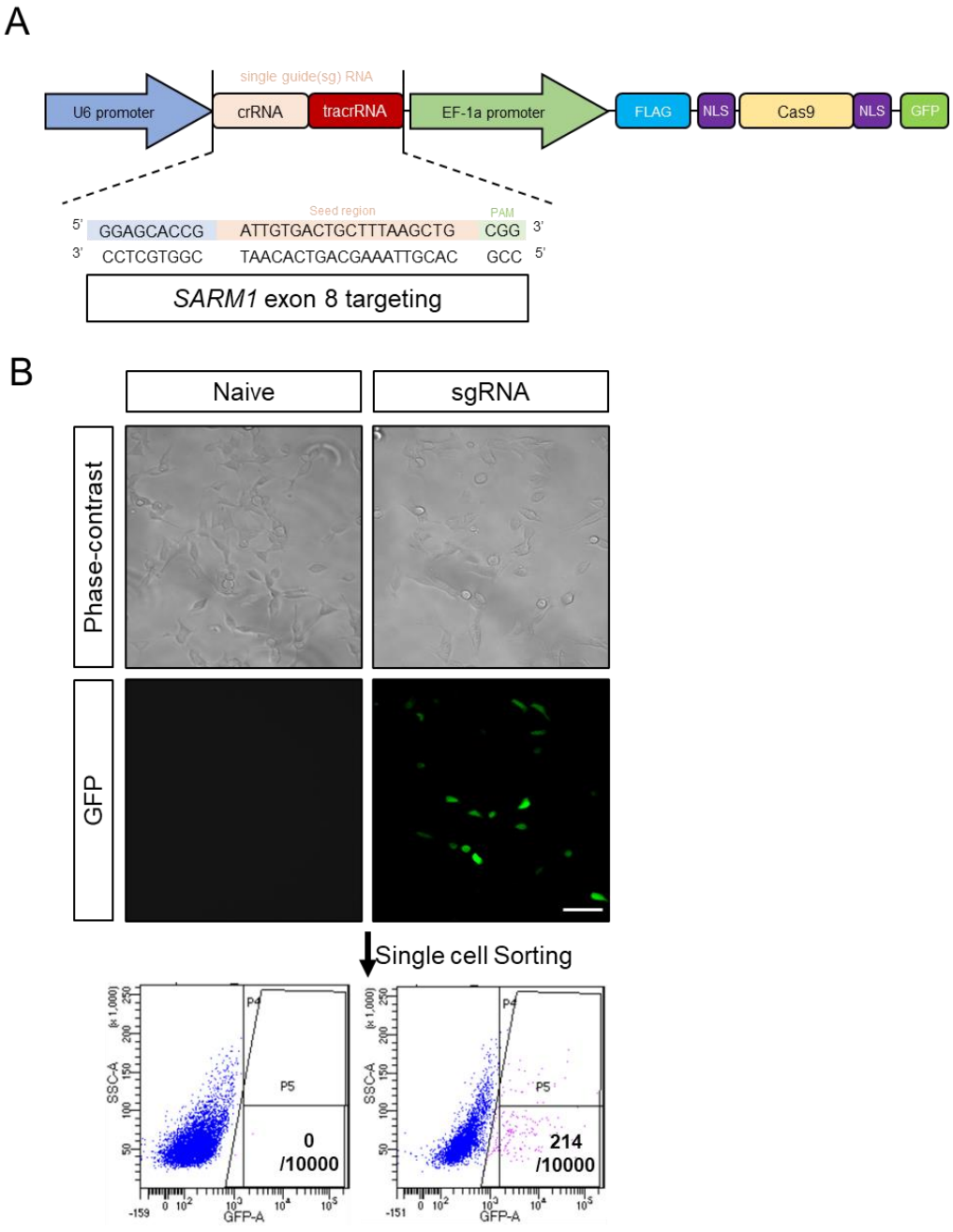

(Continued)

Figure 8. Construction of *SARM1* knockout neuronal cell line using CRISPR/Cas9. (A) Design *SARM1* sgRNA of Crispr/Cas9 expression vector for construction of *SARM1* knockout cell line. (B) Sorting of GFP-expressing cells via FACs analysis. The scale bar is 50 μm.

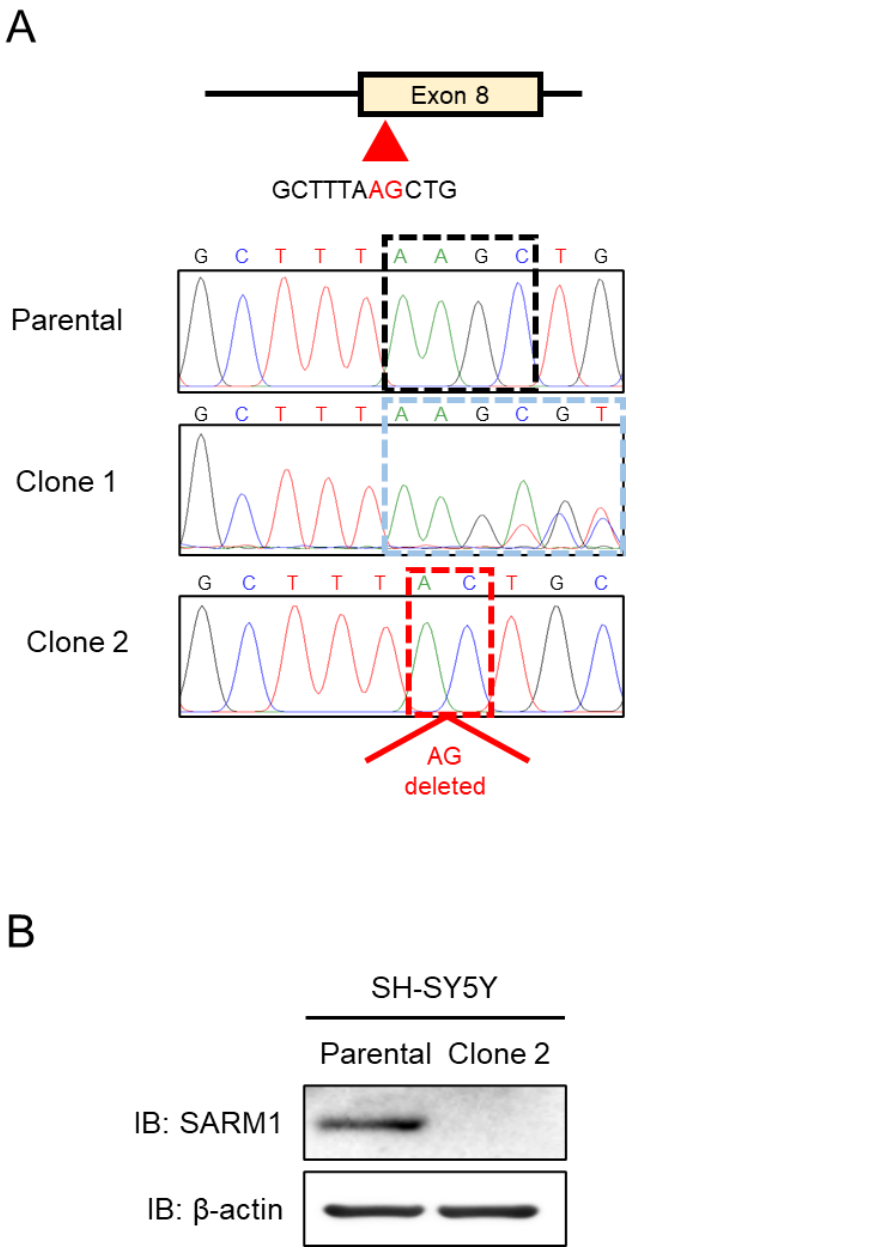

Figure 9. Selection of *SARM1* knockout clone in SH-SY5Y cell line. (A) Sanger sequencing to confirm homozygous biallelic frameshift mutations in the *SARM1* gene. (B) Western blot for confirmation of SARM1 protein expression. β-actin was loading control.

3.1.2. Establishment of cell line amenable to artificial manipulation of SARM1

In the normal state, SARM1 is maintained in an inactive state by endogenous inhibitors. Some of these inhibitors physically interact with SARM1. When SARM1 is activated, it is released from these inhibitors and interacts with new proteins to execute axon destruction.

To identify proteins that specifically interact with inactive or active SARM1, I constructed a SARM1-APEX2 fusion protein and expressed it in the *SARM1* knockout cell line obtained from the previous results. To confirm the accurate expression of the SARM1-APEX2 fusion protein, I designed a vector tagged with FLAG (Figure 10A). Additionally, for selection purposes, GFP expression under the control of the CMV promoter was incorporated into the same vector. To verify if the constructed vector was expressing normally, I transfected the SARM1-APEX2 fusion protein vector into SARM1 wild-type (WT) cells and confirmed protein expression. The expression of FLAG in transfected cells indicated the normal expression of the SARM1-APEX2 fusion protein (Figure 10B).

To assess if the expressed SARM1-APEX2 fusion protein is suitable for the APEX2 proximity biotinylation assay, I transfected *SARM1* knockout cells and conducted the APEX2 proximity biotinylation assay. Biotinylation was only observed in cells expressing the SARM1-APEX2 fusion protein, as shown in the streptavidin staining panels (Figure 11). This suggests that APEX2 proximity biotinylation specifically targeted the SARM1-APEX2 fusion protein. Consequently, I successfully validated the functionality of the SARM1-APEX2 fusion protein produced from the engineered vector.

Next, I utilized lentiviral transduction to stably express the functionally validated SARM1-APEX2 fusion protein in *SARM1* knockout cell lines. Following the transduction of *SARM1* knockout cells with lentiviral vectors, I sorted cells expressing GFP using FACs for selection purposes. Subsequently, I confirmed protein expression. While endogenous SARM1 was expressed in *SARM1* WT cells, no expression was detected in *SARM1* knockout (KO) cells. The expression of the fusion protein was confirmed in cells expressing the

SARM1-APEX2 fusion protein (Figure 12). At this stage, I selected a clone that expresses the SARM1-APEX2 fusion protein at a level comparable to that of the endogenous SARM1 protein.

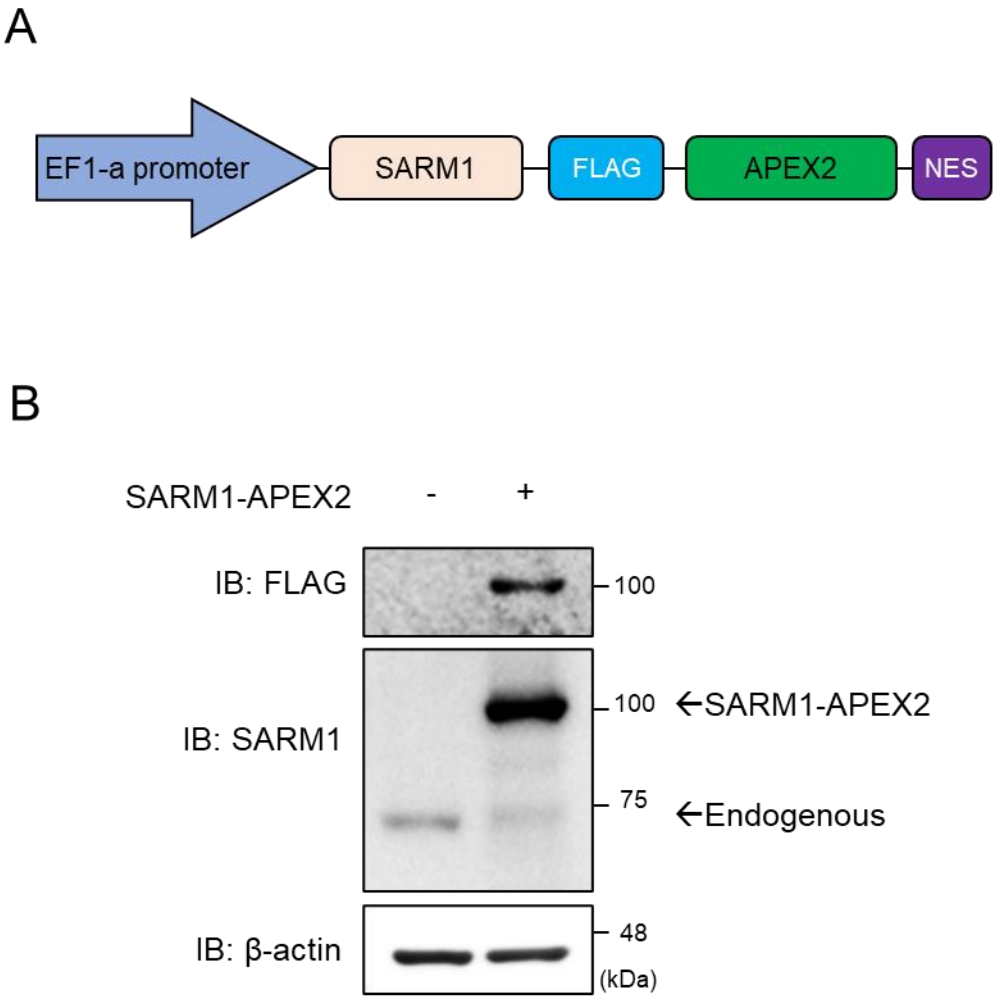

Figure 10. Expression of SARM1-APEX2 fusion protein. (A) Vector map for expressing the SARM1-APEX2 fusion protein. (B) Confirmation of SARM1-APEX2 fusion protein expression in SH-SY5Y cells via Western blot. β-actin was loading control.

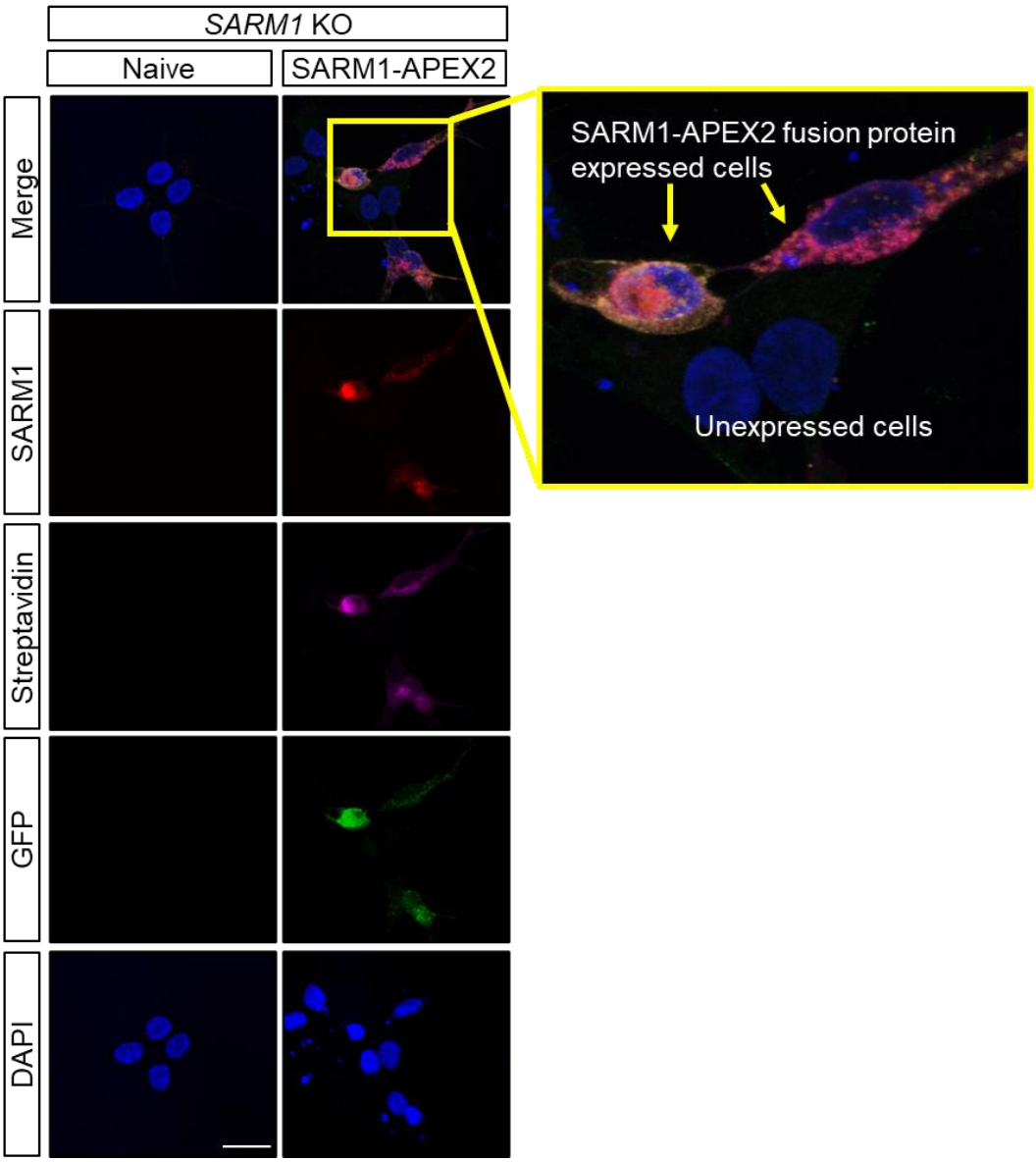

(Continued)

Figure 11. Proximity biotinylation of SARM1-APEX2 fusion protein in *SARM1* knockout cell line. SARM1-APEX2 fusion protein expression was induced, followed by proximity biotinylation. Red represents SARM1. Magenta represents streptavidin (biotinylated protein). GFP was transfection control. The yellow arrows indicate SARM1-APEX2 fusion protein expressed cells, leading to biotinylation. The scale bar is 20 μm.

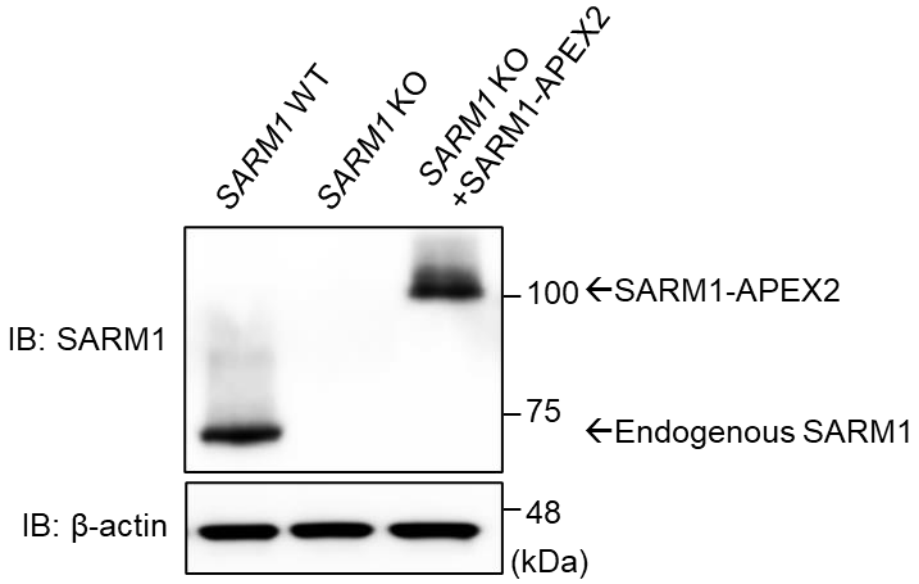

Figure 12. Establishment of a stable cell line expressing SARM1-APEX2 fusion protein in *SARM1* knockout cell line. Establishment of a cell line expressing SARM1-APEX2 fusion protein in *SARM1* knockout (KO) cell line using lentivirus. Confirmation of SARM1 expression through Western blot. β-actin was loading control.

3.1.3. The neurogenic potential and injury-induced axonal degeneration of the replaced SARM1-APEX2 fusion protein

To determine the subcellular localization and degeneration capability of the expressed SARM1-APEX2 fusion protein, I conducted the following experiments. First, to confirm the expression location compared to *SARM1* WT cells, immunocytochemistry staining was performed to visualize the expression location. Expression was observed in nearly identical locations as *SARM1* WT (Figure 13). Since SARM1 activity is induced by injury in this study, it was necessary to confirm whether degeneration occurs upon injury in the stable SARM1-APEX2 fusion protein cell line. Axotomy, or removal of the cell body, was performed using a Boyden chamber (Figure 14A). After seeding cells on the upper side of the Boyden chamber insert and inducing differentiation, ECM/laminin coating was applied to the lower side to induce axon growth. Cell bodies on the upper side were then removed using a scraper, and after 24 hours, cell nuclei (DAPI) and axons (Tuj1) were stained to confirm axon degeneration. The absence of DAPI staining after 24 hours indicated complete removal of the cell body, leading to axon fragmentation (Figure 14B). Using this method, axon degeneration experiments were conducted in three cell lines. Axon degeneration occurred in *SARM1* WT cell lines but was delayed in *SARM1* KO cell lines. Conversely, in *SARM1* KO cell lines expressing the SARM1-APEX2 fusion protein, axon degeneration and fragmentation were observed again. This confirmed that SARM1-dependent axon degeneration occurs even in cell lines replaced with SARM1-APEX2 (Figure 15).

As a result, a tool was successfully developed to identify the proximity proteins involved in SARM1-dependent axon destruction. This was achieved by creating cell lines capable of expressing the functional SARM1-APEX2 fusion protein.

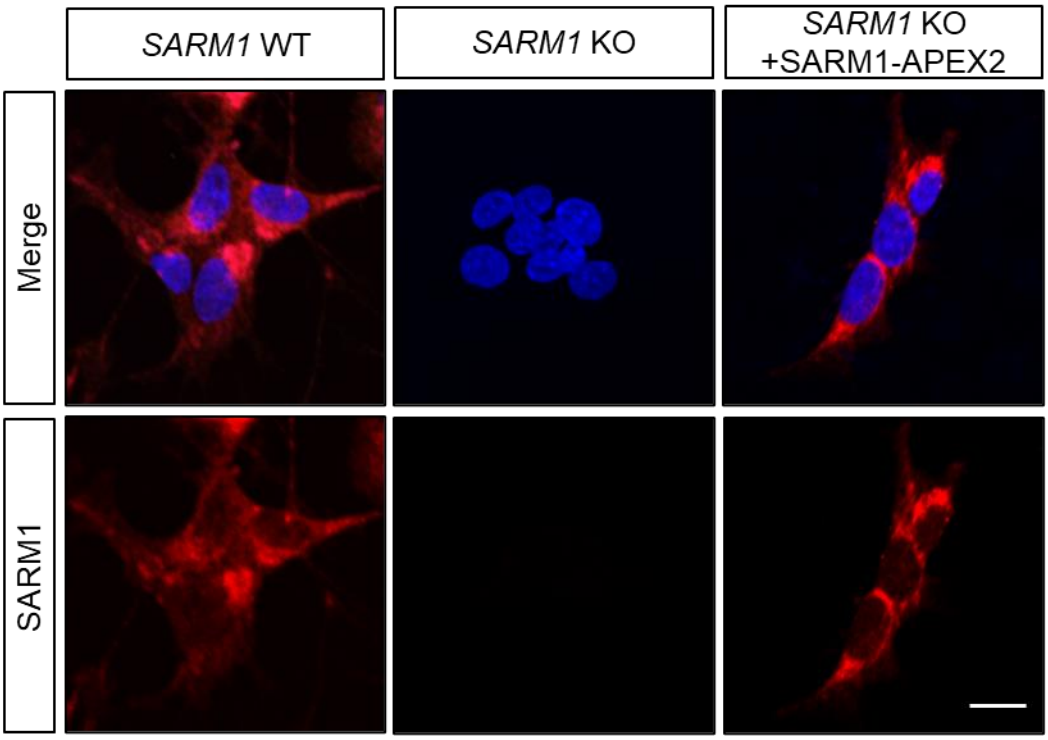

Figure 13. Localization of SARM1-APEX2 fusion protein. Expression was observed at the same location as SARM1 wild-type (WT). Red represents SARM1 and blue represents DAPI. The scale bar is 10 μm.

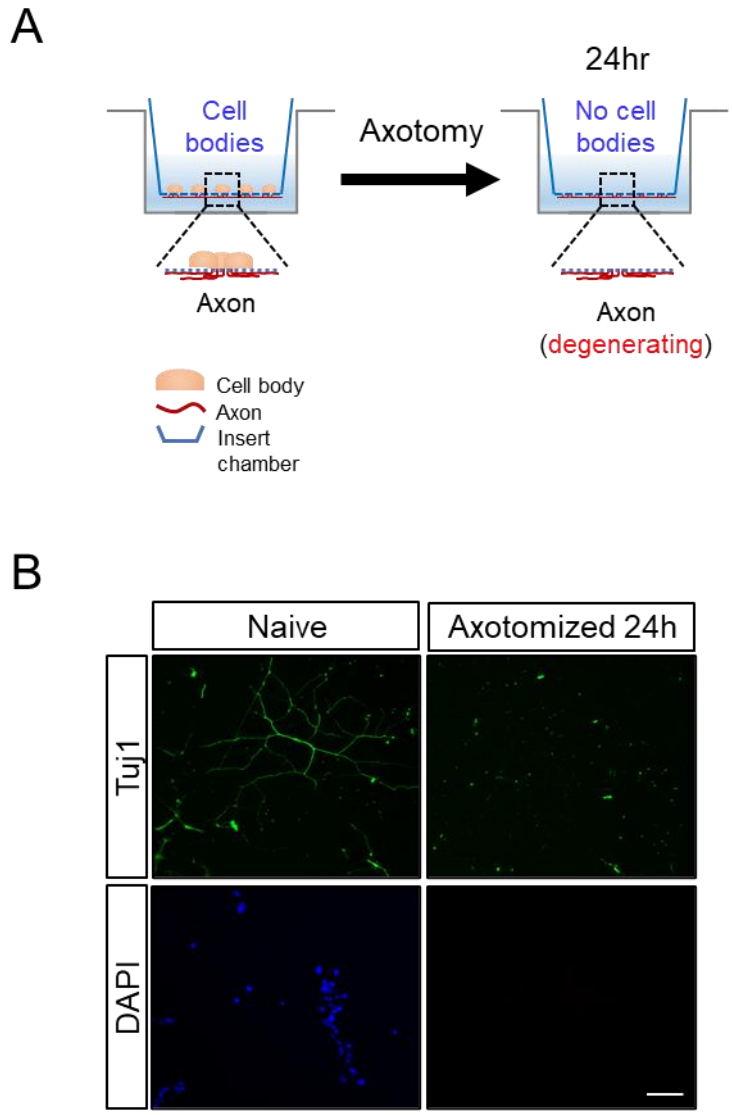

Figure 14. Investigating axon degeneration using the Boyden chamber system. (A) The Boyden chamber system enabling compartmentalized culturing of soma and axons, facilitating axotomy to selectively remove soma. (B) Axotomy was performed, and axon degeneration was confirmed 24 hours later by staining with the axonal marker Tuj1. Green represents Tuj1, and blue represents DAPI. The scale bar is 50 μm.

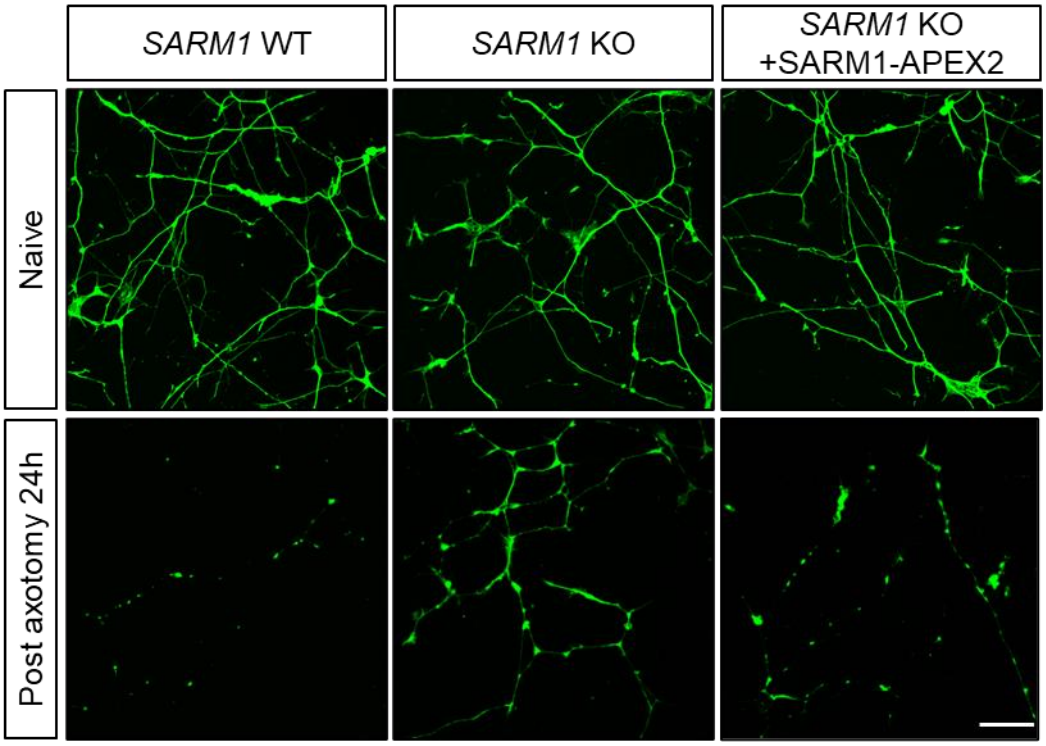

Figure 15. Functional validation of axon degeneration in differentiated SARM1-APEX2 fusion protein expressing cells. Axon degeneration induction in *SARM1* WT, *SARM1* KO, and *SARM1* KO+SARM1-APEX2 fusion protein cell lines. 24 hours post-axotomy, axon degeneration is induced in *SARM1* WT, while not observed in *SARM1* KO. However, axon degeneration occurs in the *SARM1* KO+SARM1-APEX2 fusion protein cell line, similar to *SARM1* WT. Green represents Tuj1. The scale bar is 50 μm.

3.2. Identification of activation status-dependent SARM1 proximity protein in axons

3.2.1. Verification of proximity biotinylation of SARM1-APEX2 cells in axons

To investigate protein changes induced by SARM1 activity, I successfully established a cell line expressing SARM1-APEX2 fusion protein in *SARM1* KO cells. To verify the biotinylation status at the protein level within the axons of SARM1-APEX2 fusion protein stable cells, I conducted an affinity biotinylation assay. Subsequently, to confirm whether affinity biotinylation occurs in axons post-differentiation in the SARM1-APEX2 fusion protein stable cell line, I assessed biotinylation at the protein level. For precise confirmation, I observed axons from 1 or 2 differentiated cells. In the absence of biotin-phenoxyl (BP) radicals, indicative of biotinylation, no signal was detected with avidin-A647 staining (Figure 16), despite the expression of SARM1-APEX2 fusion protein. However, treatment with BP radicals resulted in the biotinylation of proteins within ~20 nm proximity to the SARM1-APEX2 fusion protein in axons, as evidenced by avidin-A647 staining. The yellow arrowheads magnified in the panel from cells treated with BP radicals visualize proteins biotinylated near the SARM1-APEX2 fusion protein, which I aimed to identify through further characterization and protein identification.

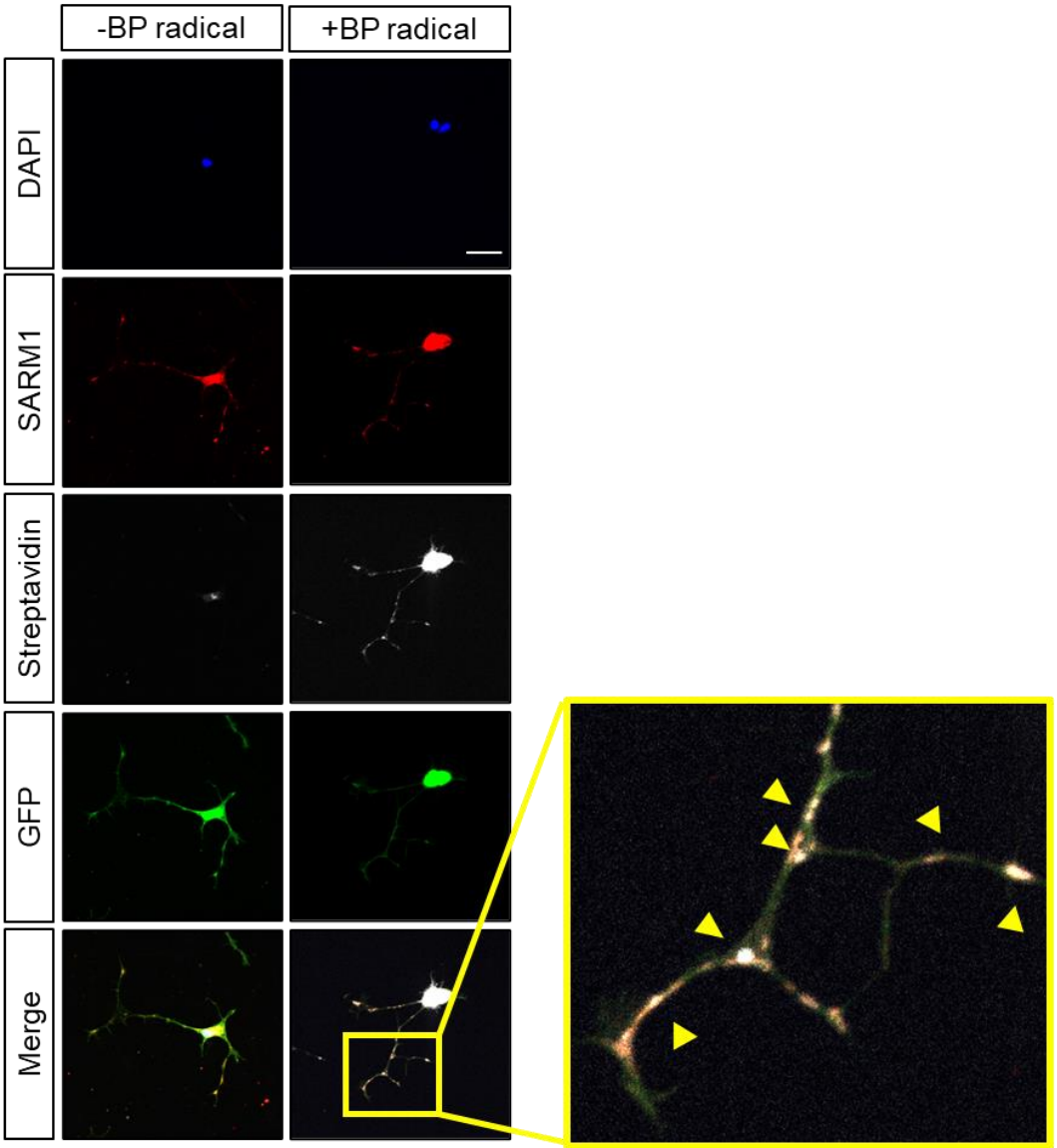

(Continued)

Figure 16. Proximity biotinylation by SARM1-APEX2 in axons. In the group treated with BP radicals, only biotinylated proteins are visualized in the *SARM1* KO+SARM1-APEX2 fusion protein stable cell line. Red represents SARM1, white represents streptavidin-A647 (biotinylated protein), and blue represents DAPI. The scale bar is 50 μm.

3.2.2. Feasibility of affinity purification and enrichment of biotinylated proteins

I visualized protein-level biotinylation in the *SARM1* KO+SARM1-APEX2 fusion protein stable cell line. Each cell line was treated with BP radical, and I confirmed proximity biotinylation through Western blotting to visualize biotinylated proteins. I performed Ponceau S staining on the same membrane to verify only biotinylated proteins through proximity biotinylation assay from equal amounts of the same protein. No biotinylated proteins were observed when BP radical was applied to *SARM1* WT cells or *SARM1* KO cells. Additionally, in the *SARM1* KO+SARM1-APEX2 fusion protein cell line, biotinylated proteins were not generated without BP radical treatment. However, biotinylated proteins were only observable through streptavidin staining when treated with BP radical (Figure 17A), confirming successful biotinylation through APEX2 proximity biotinylation assay in the *SARM1* KO+SARM1-APEX2 fusion protein cell line.

Next, I attempted to specifically identify biotinylated proteins through a proximity biotinylation assay. I performed immunoprecipitation using streptavidin-beads in the lysate of a *SARM1* KO+SARM1-APEX2 fusion protein stable cell line to enrich biotinylated proteins. I observed the enrichment of biotinylated proteins only from cells treated with BP radical during immunoprecipitation (Figure 17B). Through this method, I successfully demonstrated proximity biotinylation throughout the entire cell and validated the feasibility of affinity purification by selectively enriching biotinylated proteins.

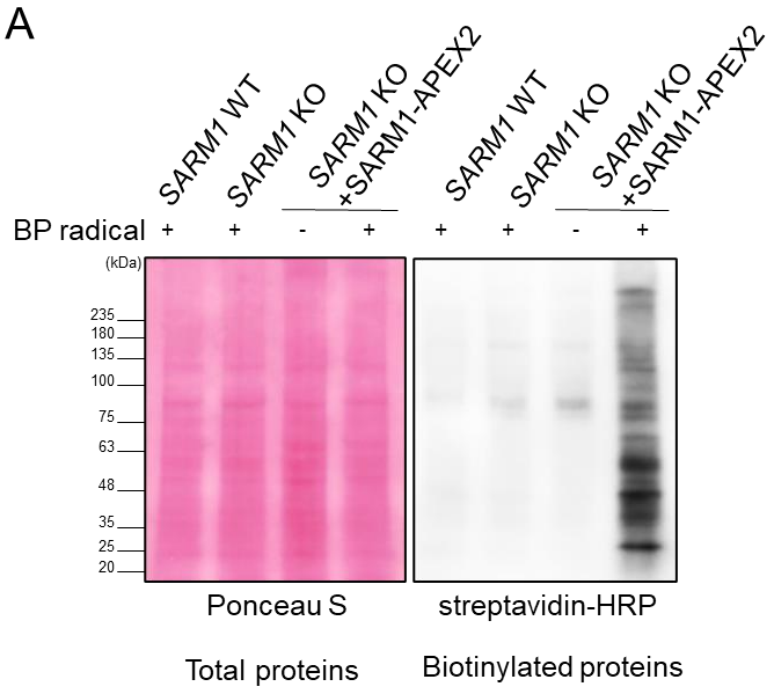

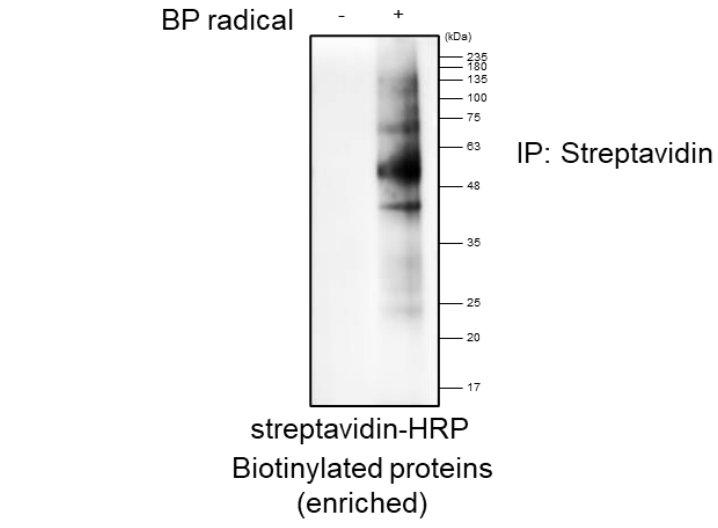

(Continued)

Figure 17. Purification and enrichment of biotinylated proteins through APEX2 proximity biotinylation in whole cells. (A) Western blot analysis of biotinylated proteins following proximity biotinylation in *SARM1* WT, *SARM1* KO, and *SARM1* KO+SARM1-APEX2 fusion protein stable cell lines. The left panel shows Ponceau S staining for total protein loading control. The right panel shows biotinylated proteins detected using streptavidin-HRP. (B) Biotinylated proteins were immunoprecipitated using streptavidin to enrich for proteins based on the presence or absence of BP radical in the *SARM1* KO+SARM1-APEX2 fusion protein stable cell line.

3.2.3. Identification of relevant proteins through affinity purification and LC-MS/MS analysis of biotinylated proteins in naive axons and injured axons

To investigate changes in the proximity proteins due to SARM1 activation in the axon, it was necessary to isolate axons and conduct experiments exclusively on them. To conduct the experiment, it was imperative to determine the time frame after axotomy when the signaling of the axon destruction program initiates. Consequently, it was confirmed that this signaling begins 1 hour after axotomy. The reason for obtaining axon proteins 1 hour after axotomy is twofold. Firstly, within 4 hours after injury, irreversible axon destruction proceeds, known as the latent phase [25]. Morphologically intact axons exist during this period, but calcium influx occurs within 1 hour in injured axons. Secondly, SARM1 activation induces axon degeneration, and p-JNK, one of the injury response signals, is known to be activated concurrently with SARM1 activation [26-28]. In actual experimentation, the expression of p-JNK peaked 1 hour after axotomy and decreased by 3 hours, indicating that SARM1 activation occurred within or before the 1 hour (Figure 18).

I established two groups (Figure 19A). Group 1 comprised naive axons subjected to proximity biotinylation, while group 2 consisted of injured axons at 1 hour after removal of the cell body, and subjected to affinity biotinylation.

In both groups, cell bodies and axons were compartmentalized using a Boyden chamber, and proximity biotinylation was performed to isolate only the axons. Affinity purification on the isolated axons confirmed the presence of biotinylated proteins within the axons, visualized by streptavidin-HRP on Western blots. Successful enrichment was achieved for further analysis (Figure 19B). The enriched proteins were identified using mass spectrometry to determine the protein composition present within the axons.

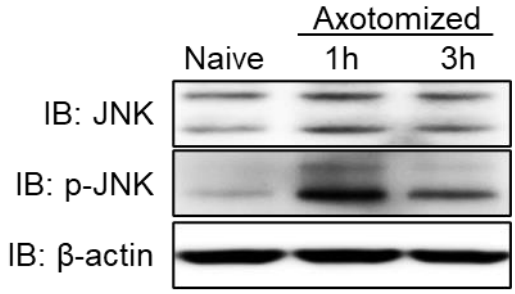

Figure 18. JNK signaling in axotomized axons. Expression of JNK and p-JNK in damaged axons using Western blot. β-actin was loading control.

A

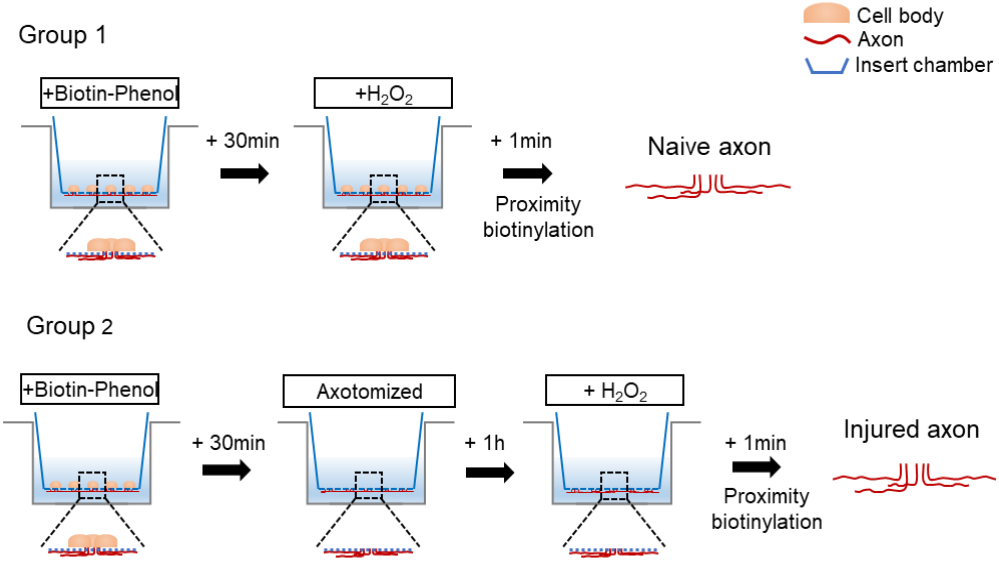

B

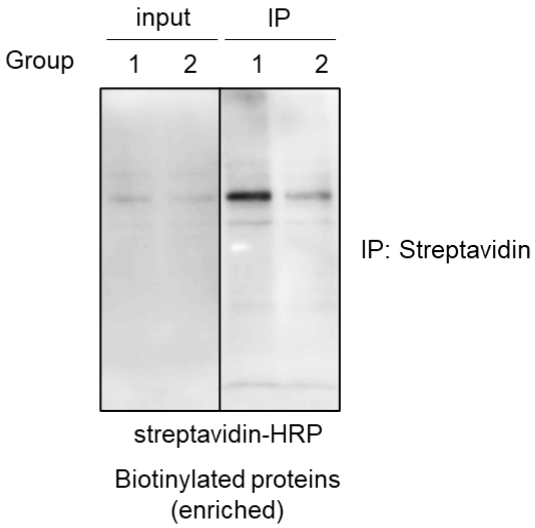

(Continued)

Figure 19. Affinity purification of biotinylated proteins naive axon and injured axons. (A) Overview of the analysis groups. (B) Affinity purification of biotinylated proteins from axons of Group 1 and Group 2 using streptavidin-beads.

Through mass analysis, I was able to identify a diverse range of proteins. A total of 1075 proteins were identified, of which 23 proteins (2% of the total) were exclusive to naive axons, while 27 proteins (3% of the total) were exclusive to injured axons. Additionally, within the intersection of the two groups, proteins were identified that were highly expressed in either naive axons or injured axons, as shown in the Venn diagram (Figure 20). A list of proteins uniquely identified in naive axons (Table 1) and those uniquely identified in injured axons (Table 2) was enumerated. Thus, I successfully identified the proximity proteins of the SARM1-dependent axon destruction program for the first time and provided a list of proteins.

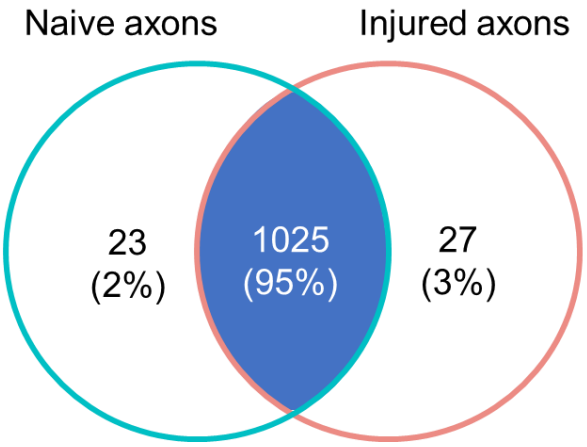

Figure 20. The Venn diagram of protein counts derived from mass spectrometry analysis. The Venn diagram showing the proteins interacting with naive axons (23 proteins), injured axons (27 proteins), or both (1025 proteins).

Table 1. List of proteins uniquely identified in naive axons

Protein	Gene Symbol
Keratin, type I cytoskeletal 16	KRT16
Protein tweety homolog 3	TTYH3
Prolyl endopeptidase	PREP
Phosphatidate cytidylyltransferase 2	CDS2
GDNF family receptor alpha-2	GFRA2
Ribose-phosphate pyrophosphokinase 2	PRPS2
Keratin, type II cuticular Hb1	KRT81
Glucose-6-phosphate isomerase	GPI
14 kDa phosphohistidine phosphatase	PHPT1
Aldehyde dehydrogenase 1A1	ALDH1A1
Electron transfer flavoprotein subunit alpha, mitochondrial	ETFA
Aldehyde oxidase	AOX1
Junctional adhesion molecule C	JAM3
Neogenin	NEO1
Isoform 2 of Isocitrate dehydrogenase subunit gamma, mitochondrial	IDH3G
Prostaglandin F2 receptor negative regulator	PTGFRN
Protein ZNF365	ZNF365
Mitochondrial import inner membrane translocase subunit Tim23	TIMM23
Secretogranin-2	SCG2
Kinesin-like protein KIF3A	KIF3A
Calmodulin-regulated spectrin-associated protein 3	CAMSAP3
Serine/threonine-protein phosphatase 2A 56 kDa regulatory subunit beta isoform	PPP2R5B
Coiled-coil alpha-helical rod protein 1	CCHCR1

Table 2. List of proteins uniquely identified in injured axons

Protein	Gene Symbol
Ski oncogene	SKI
Filamin-C	FLNC
Malate dehydrogenase, mitochondrial	MDH2
Integrin alpha-7	ITGA7
Small ribosomal subunit protein uS2B	RPSA2
Neurexin-2	NRXN2
Hsc70-interacting protein	ST13
Serine/threonine-protein kinase Nek9	NEK9
Thioredoxin domain-containing protein 17	TXNDC17
Splicing factor 3B subunit 3	SF3B3
Enoyl-CoA hydratase, mitochondrial	ECHS1
Retinol-binding protein 1	RBP1
Nucleosome assembly protein 1-like 1	NAP1L1
Drebrin-like protein	DBNL
Glypican-1	GPC1
Isoform 5 of SH3-containing GRB2-like protein 3-interacting protein 1	SGIP1
DnaJ homolog subfamily A member 1	DNAJA1
Parkinson disease protein 7	PARK7
Transketolase	TKT
Caspase recruitment domain-containing protein 6	CARD6
BolA-like protein 2	BOLA2; BOLA2B
Diphosphoinositol polyphosphate phosphohydrolase 2	NUDT4
Ubiquitin carboxyl-terminal hydrolase 14	USP14
Cancer-related nucleoside-triphosphatase	NTPCR
Serotransferrin	TF
Multivesicular body subunit 12A	MVB12A
Jupiter microtubule associated homolog 2	JPT2
Ethanolamine-phosphate cytidylyltransferase	PCYT2

3.3. Functional analysis of SARM1 proximity proteins

I have identified the proximity protein of the SARM1-dependent axon destruction program in axons upon the activation and deactivation of SARM1. I am confident that my data can offer insights into the following aspects.

First, I anticipate that Gene Set Enrichment Analysis, I can determine whether the localization of SARM1 changes within the first hour of activation. Second, by analyzing proteins specifically bound after SARM1 activation, I may identify executors or co-factors involved in its activation process.

3.3.1. Gene Set Enrichment Analysis on changes in proximity proteins after injury

I utilized Gene Set Enrichment Analysis (GSEA) to assess changes observed in the data acquired through mass spectrometry. GSEA is an analytical technique employed to understand the biological significance of gene sets. This method evaluates whether sets of genes or proteins are associated with specific biological processes, cellular organelles, pathological conditions, or other biological categories. Typically, a gene or protein set is considered "enriched" when it is statistically significantly associated with a particular biological category under specific conditions. Gene set enrichment analysis is recognized as a valuable tool for comprehending and interpreting complex genomic data [29].

After classifying approximately 1000 proteins based on the extent of their increase following injury, those showing significant increases were listed on the left, while those exhibiting decreases were listed on the right. Subsequently, I evaluated whether known genes associated with each pathway showed an increase or decrease. Various pathways were found to be enriched, indicating diverse pathway activation in injured axons (Figure 21). Here are the interpretations of the results.

Firstly, proteins enriched in autophagy (Figure 22A), cellular responses to chemical stress

(Figure 22B) and stimuli (Figure 22C) showed significant values. This suggests that stress and degradation programs are rapidly activated within the axon within the first hour post-injury, indicating ongoing axon degeneration.

Secondly, a decrease in mitochondrial protein levels was observed, particularly in the citric acid (TCA) cycle (Figure 23A) and respiratory electron transport (Figure 23B), indicating mitochondrial dysfunction. Based on these results, I conducted Gene Set Enrichment Analysis (GSEA) using cellular component terms of the Gene Ontology (GO) database (Figure 24). Notably, I observed a decrease in mitochondrial association (Figure 25A). However, intriguingly, there was an increasing trend in actomyosin association (Figure 25B). This suggests the possibility that SARM1, which was either bound to or in close proximity to mitochondria, may dissociate from there upon activation by injury. Additionally, it suggests the possibility that SARM1 may be docked at the mitochondria and leave upon activation. In other words, this implies that inactive SARM1 may be associated with mitochondria and could relocate upon activation.

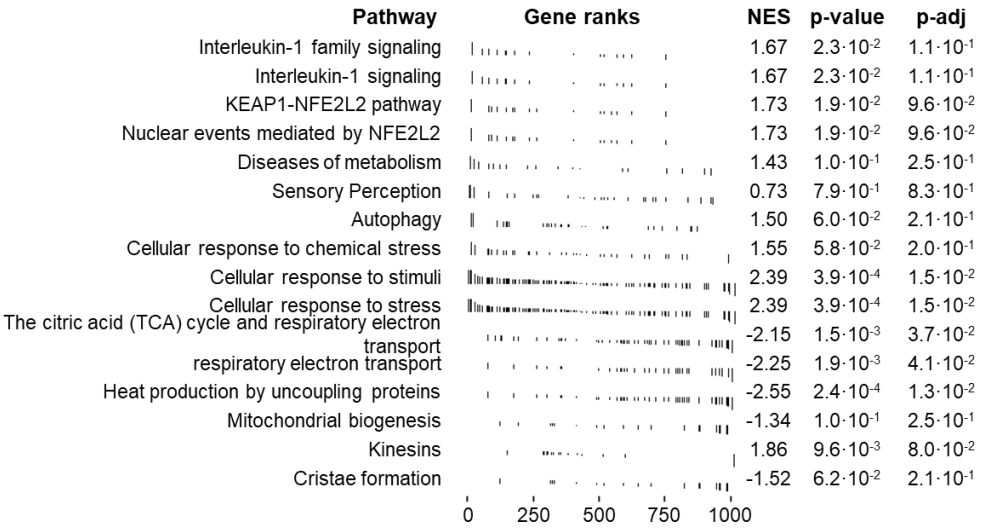

Figure 21. Gene set enrichment analysis (Reactome pathways). Gene set enrichment analysis of naive axons vs injured axons. NES: normalized enrichment scores. p-value: probability value. p-adj: false discovery rate (FDR)-adjusted p value.

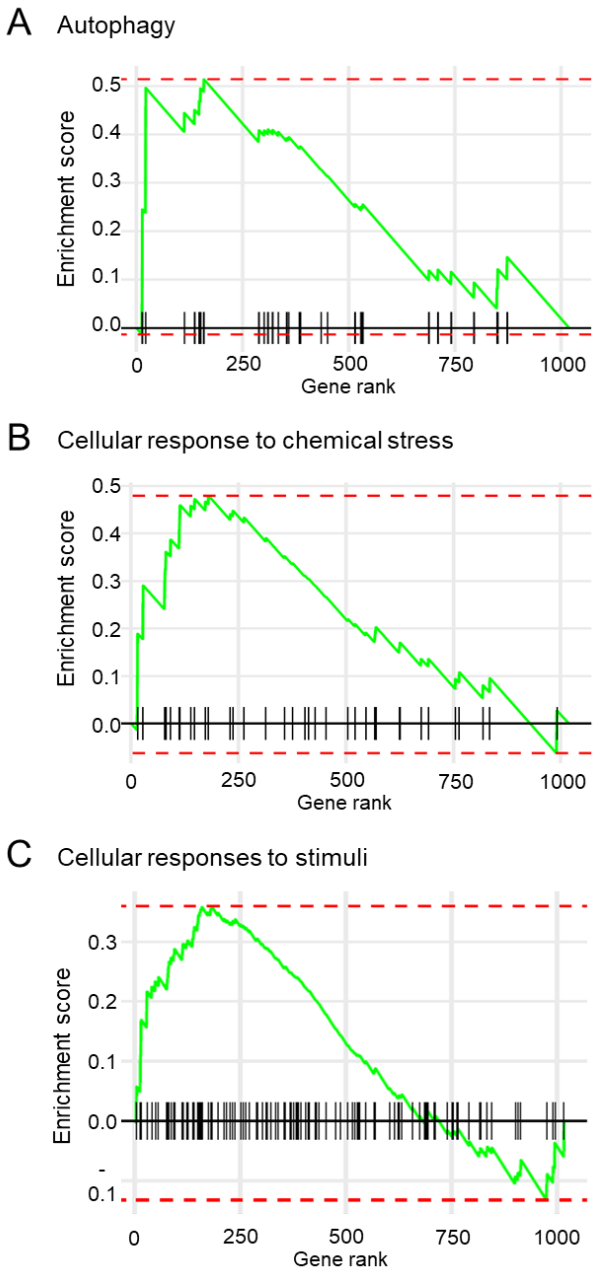

Figure 22. Enrichment plot of the upregulated pathway. (A) Autophagy. (B) Cellular response to chemical stress. (C) Cellular responses to stimuli.

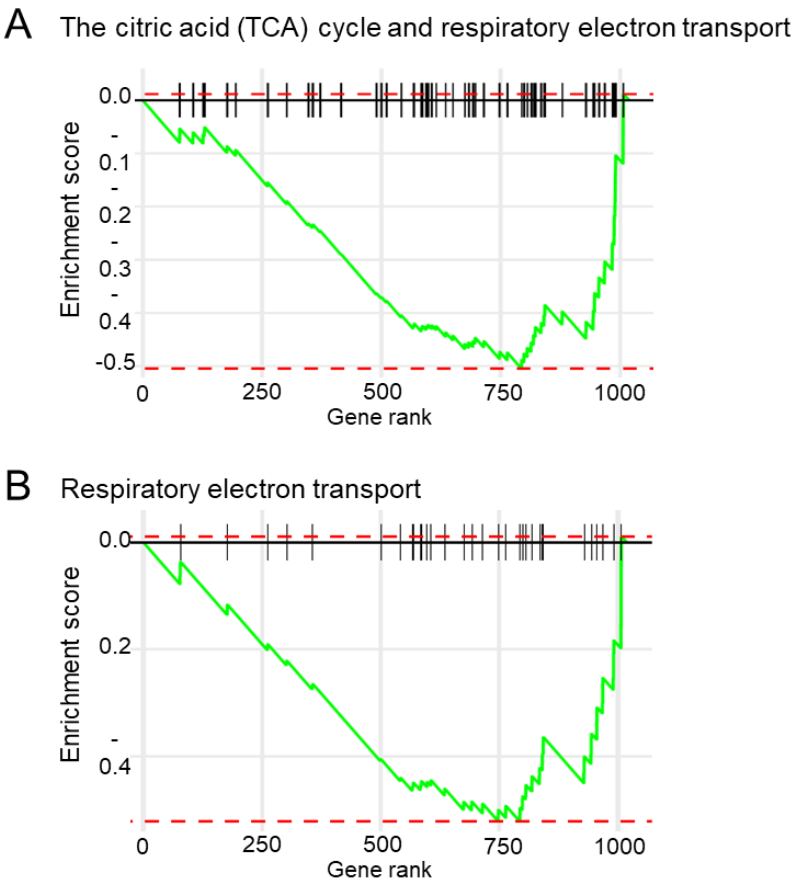

Figure 23. Enrichment plot of the downregulated pathway. (A) The citric acid (TCA) cycle and respiratory electron transport. (B) Respiratory electron transport.

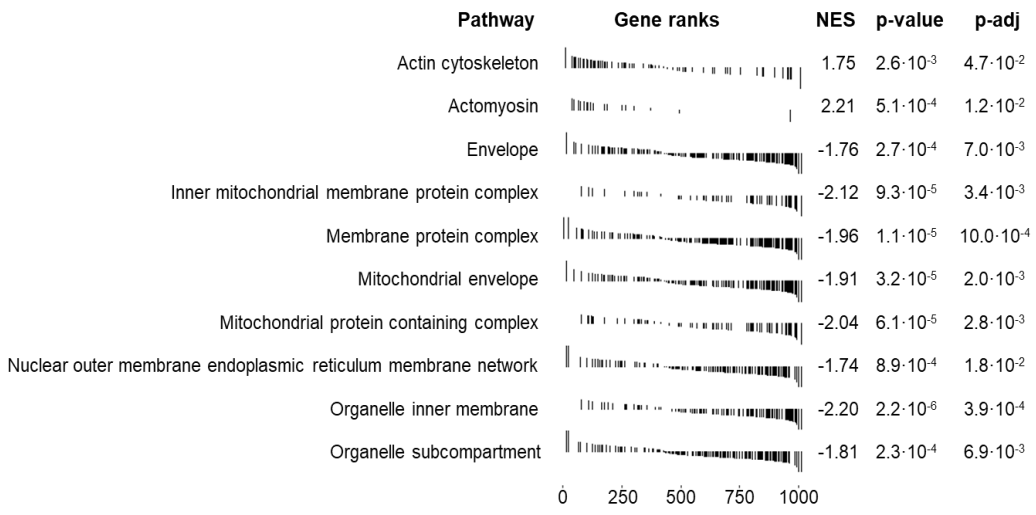

Figure 24. Gene set enrichment analysis (Gene Ontology Terms: Cellular Component). Gene set enrichment analysis using cellular component gene ontology terms of naive axons vs injured axons. NES: normalized enrichment scores. p-value: probability value. p-adj: false discovery rate (FDR)-adjusted p value.

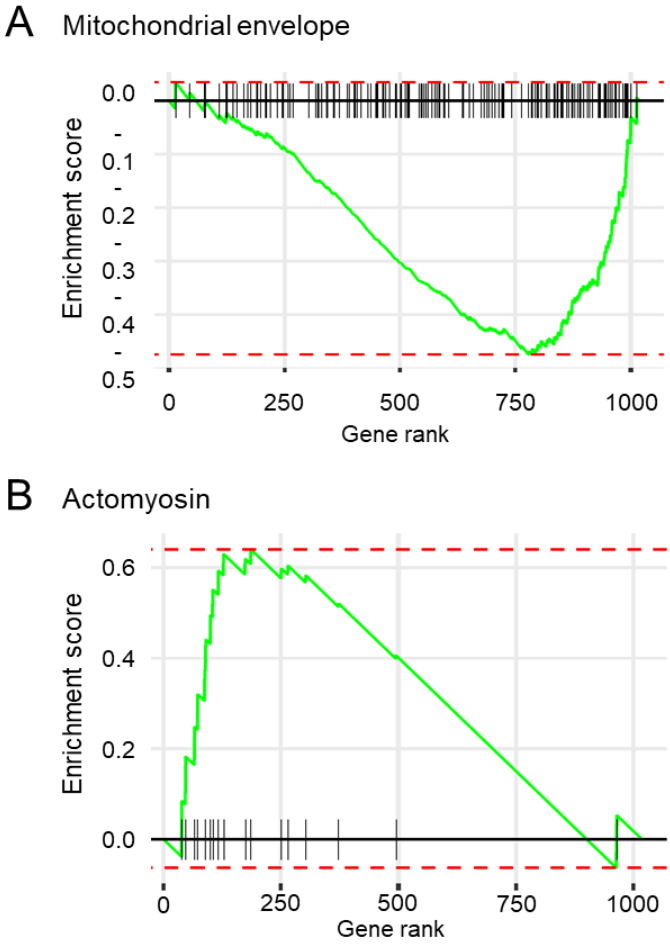

Figure 25. Enrichment plot of cellular component terms. (A) Mitochondrial envelope. (B) Actomyosin.

3.3.2. Potential facilitator of SARM1 activation

As a result of mass spectrometry, proteins involved in NAD^+ metabolism were identified among the known pathway proteins. One protein that was more frequently detected around the early stages of activated SARM1 compared to inactive SARM1 was Nicotinamide phosphoribosyltransferase (*NAMPT*). Although not statistically significant, it exhibited substantial increases on a log scale (Figure 26A). The significance of the higher frequency of NAMPT detection around the early stages of activated SARM1 implies the potential clustering of NAMPT around SARM1 during the initial SARM1 activation stage. This suggests that the role of NAMPT may occur much earlier in the preparatory stage for axonal degeneration before complete axonal degeneration occurs.

NAD^+ consumed by SARM1 generates nicotinamide (NAM), which is converted to nicotinamide mononucleotide (NMN) by Nicotinamide phosphoribosyltransferase (NAMPT). NMN is then reduced back to NAD^+ by Nicotinamide mononucleotide adenylyltransferase 1-3 (NMNAT1-3), and this process is known as the salvage pathway. It is understood that NMN itself can activate SARM1, while NAD^+ inhibits SARM1 (Figure 26B) [30-33]. Homeostasis of the NMN-to-NAD^+ ratio acts as an important factor in axon degeneration [5, 34, 35]. Research is being conducted targeting many enzymes in the NAD^+ pathway, and among them, NAMPT inhibitors have received attention for offsetting the side effects of neuropathy caused by chemotherapy, and are particularly attracting attention as a treatment for truncated Wallerian degeneration that depends on SARM1 activation [36, 37].

In this context, inhibition of NAMPT suppresses SARM1, thereby delaying axon degeneration. This minor delay occurs because eventually, without NMN, NAD^+ levels decrease. Concurrently, as part of the development of novel anticancer agents, a new NAMPT inhibitor has been developed. The newly developed inhibitor, A4276, reduces NMN levels, but to a lesser extent. Experimental comparisons were conducted between these inhibitors and the existing NAMPT inhibitor, FK866 [33, 38, 39]. The drugs were administered to *Xenopus tropicalis* embryos for 48 hours, and the concentrations of NAD^+ and NMN were measured using mass spectrometry. Both inhibitors decrease NMN levels, but A4276

preserves NAD^+ levels to a greater extent relative to FK866 (Figure 27A).

To evaluate whether the newly developed drug is more effective in delaying Wallerian degeneration than the existing drug, I conducted two experiments.

First, I visualized only the optic nerve in a living *Xenopus tropicalis* brain using axon tracing technique. GFP was electroporated into retinal ganglion cells of *Xenopus tropicalis* to fluorescently tag the retinal cells. After axotomy, Wallerian degeneration occurred, as indicated by axon fragmentation after 48 hours. The previously known drug FK866 delayed degeneration but did not prevent it. This is attributed to the eventual reduction in NAD^+ levels. However, treatment with the A4276 drug preserved NAD^+ and decreased NMN, thereby delaying the activation of SARM1 and resulting in significant axonal protection (Figure 27B).

Second, to validate these findings in another model, I cultured sensory neurons from mice and induced axon degeneration using the same Boyden chamber system after axotomy. After 24 hours, Wallerian degeneration occurred, as evidenced by axon fragmentation. However, when treated with A4276, axonal degeneration was significantly delayed (Figure 28). This was further supported by measuring the axon fragmentation index, demonstrating that A4276 is the most potent drug in preventing axonal degeneration observed to date. These results suggest that the newly developed drug A4276 may be more effective in delaying Wallerian degeneration compared to the existing drug FK866.

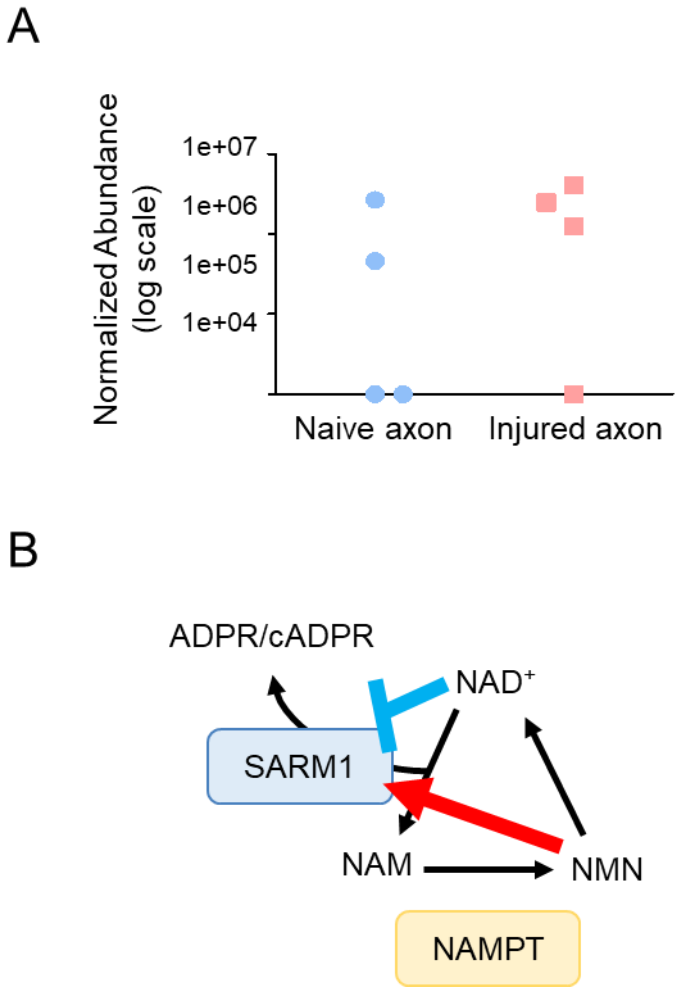

Figure 26. Potential Facilitator of SARM1 Activation: NAMPT. (A) Normalized abundance graph of NAMPT obtained through mass spectrometry. (B) Correlation between SARM1 and the NAD^+ pathway.

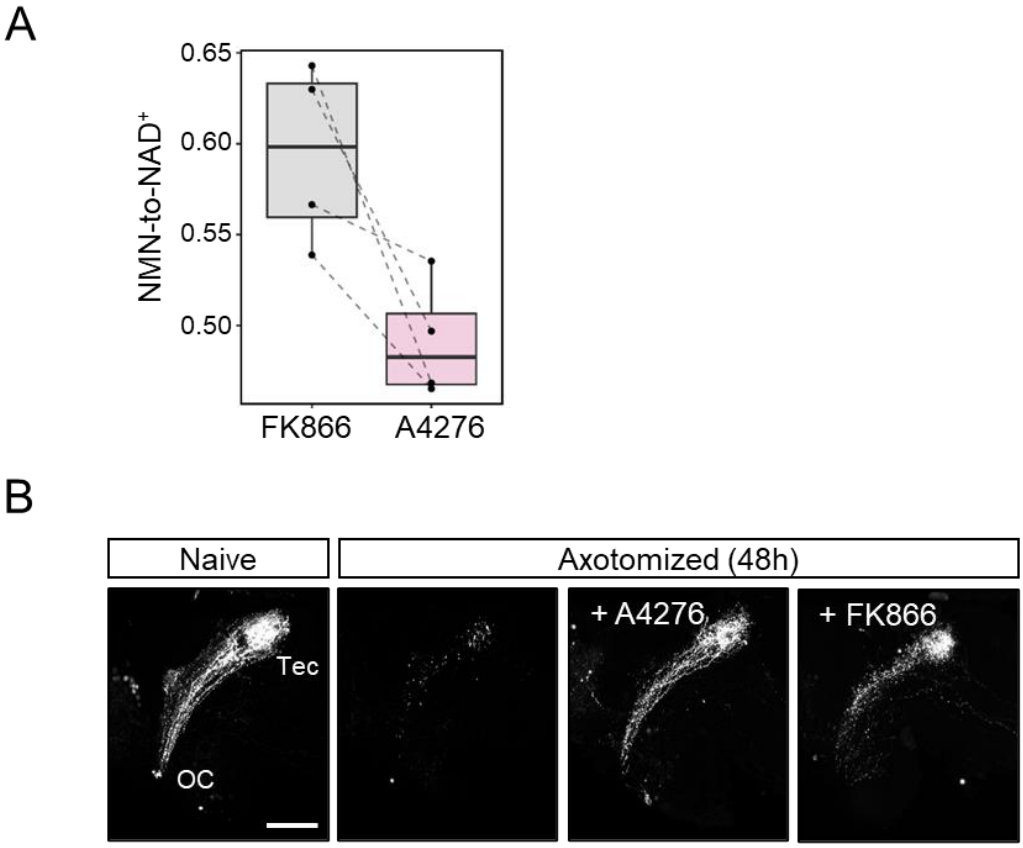

Figure 27. Verification of the delaying effect of the drug A4276 on Wallerian degeneration in *Xenopus tropicalis*. (A) The NMN-to-NAD$^+$ ratio of FK866 and A4276, NAMPT inhibitors. (B) After optic nerve transection in *Xenopus tropicalis*, treatment with A4276 (10 μM) and FK866 (10 μM) was administered. After 48 hours of axotomy, successful delay of Wallerian degeneration was observed in the A4276 treatment group, while FK866 showed mild delay. OC: optic chiasm. Tec: tectum. The scale bar is 50 μm.

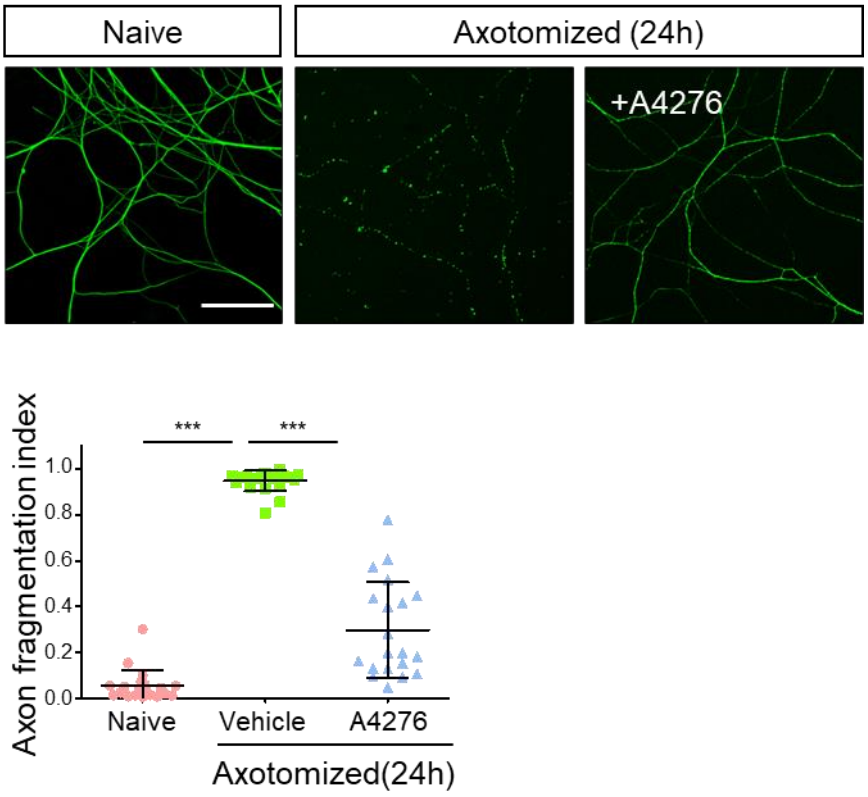

Figure 28. Verification of the delaying effect of the drug A4276 on Wallerian degeneration in mouse DRG neurons. Immunocytochemical images display the acetylated alpha-tubulin in mouse DRG neurons after 24 hours of axotomy. Treatment with A4276 (2 μM) is shown to delay Wallerian degeneration. Axon degeneration was quantified, with ***$p < 0.001$ indicating significance. Statistical analysis was conducted using ordinary one-way ANOVA, followed by Bonferroni's multiple comparisons tests. The data is presented as mean ± standard deviation (n = 20 each). Scale bar: 50 μm.

As previously mentioned, since Wallerian degeneration and various degenerative diseases share almost the same mechanism, I conducted these experiments to determine if this drug could prevent dying-back.

Chemotherapy-induced peripheral neuropathy (CIPN) represents a significant clinical condition that requires medications to alleviate Wallerian degeneration. CIPN, a common side effect of chemotherapy, is characterized by the development of painful neuropathy during drug administration and the degeneration of highly myelinated primary sensory axons, leading to a permanent loss of tactile sensation. Due to the notable effectiveness of A4276 in delaying Wallerian degeneration in dorsal root ganglion (DRG) neurons and reducing CIPN symptoms, I conducted a study to explore the potential of this drug in preventing CIPN.

Mouse DRG neurons were cultured in a microfluidic device with soma and axonal compartments separated. To model CIPN, the chemotherapeutic drugs vincristine (Figure 29A) and paclitaxel (Figure 29B), associated with CIPN, were administered to the axonal compartment. Co-treatment of both chemotherapeutic agents and A4276 resulted in delayed degeneration compared to the group treated with chemotherapeutic drugs alone, as evidenced by the axon fragmentation index. Under these culture conditions, treatment with A4276 alongside chemotherapeutic drugs prevented chemotherapy-induced axonal degeneration. [21].

In conclusion, my data clearly demonstrate that co-treatment of A4276 with chemotherapeutic drugs can delay the onset of CIPN. This underscores the potential utility of A4276 as a promising option for combination therapy in cancer treatment and highlights its significance as a drug that inhibits Wallerian degeneration. This content was published in 2023 in *Theranostics*, with me as the first author [21].

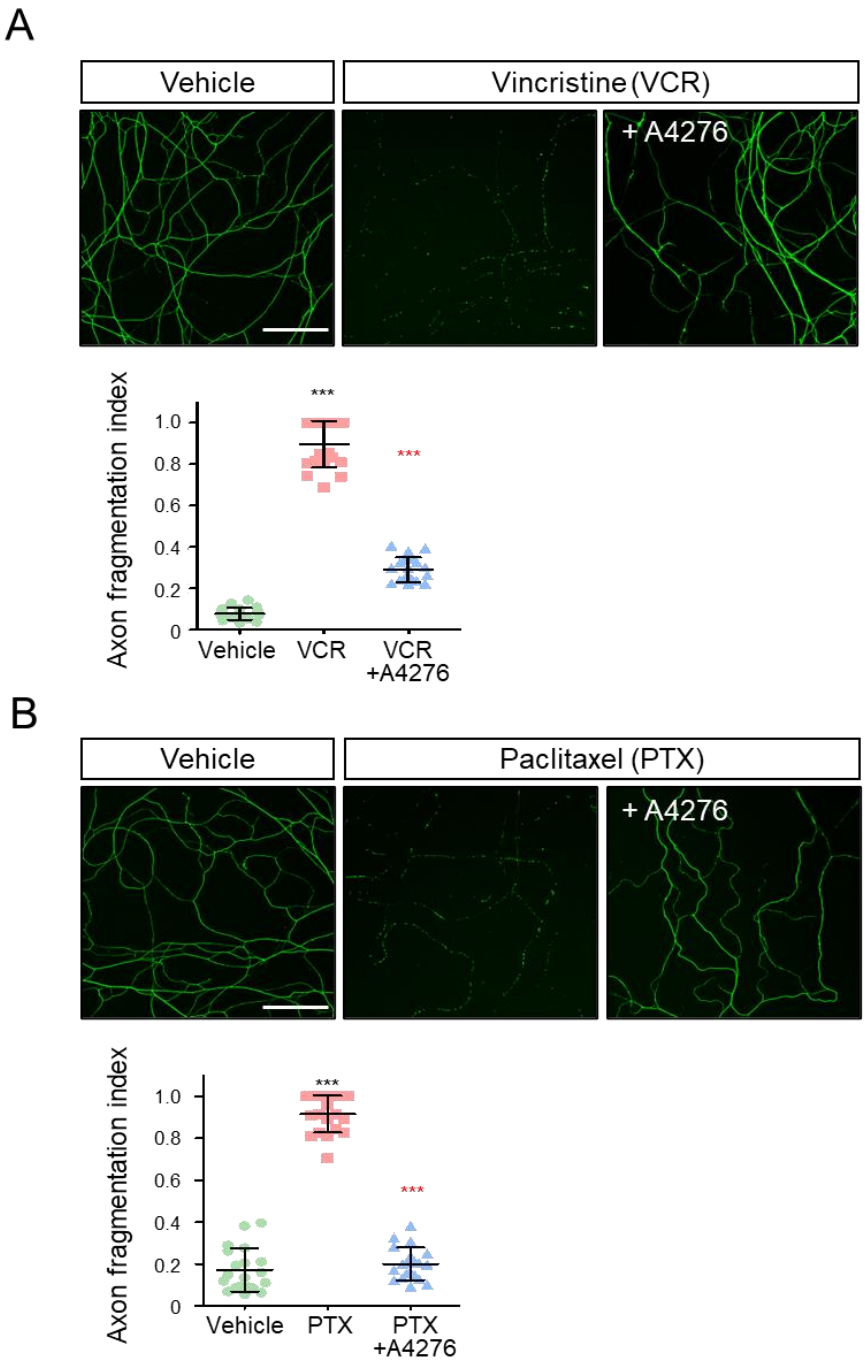

(Continued)

Figure 29. A4276 delays chemotherapy-induced axon degeneration. Immunocytochemical images display acetylated alpha-tubulin after treatment with either 40 nM vincristine (A) or 100 nM paclitaxel (B), with or without of 2 μM A4276H. Axonal degeneration was quantified. The statistical analysis revealed ***$p < 0.001$. Statistical significance was determined using ordinary one-way ANOVA followed by Bonferroni's multiple comparisons test; data are presented as mean ± SD (n = 20 per group).

4. Discussion

In this study, I successfully identified changes in proximity proteins for the first time through the SARM1-dependent axon degeneration program in both normal and damaged axons. Specifically, I separated and identified proximity proteins associated with early SARM1 activation, contributing to the elucidation of the molecular mechanisms underlying SARM1's autoinhibition and activation in axons. The results of this study revealed the identification of molecules associated with SARM1 in the process of axon degeneration, expanding and strengthening the existing dataset by adding new discoveries to known SARM1-associated proteins. Furthermore, by demonstrating the association of molecules inducing axon degeneration with SARM1, which plays a central role in the axon degeneration program, I can suggest the possibility of new signaling pathways.

As a result, I have demonstrated that mitochondrial dysfunction accompanies the activation of the axon degeneration program. This supports the significant impact of known mitochondrial dysfunction on the survival of neurons [40-44]. Interestingly, the analysis of identified proteins revealed evidence of changes in the intracellular localization of the SARM1 protein in response to injury. According to Gene Set Enrichment Analysis (GSEA), there was an increase in stress responses (autophagy, cellular response to chemical stress and stimuli) and a decrease in mitochondrial proteins (citric acid cycle and electron transport chain). Axon degeneration induced by mitochondrial dysfunction is a well-known fact, indicating a strong association with mitochondria. Previous studies have suggested the possibility of SARM1 translocating to the mitochondrial membrane, and research on the role of SARM1 within mitochondria is gaining attention [10, 45-48]. SARM1 contains an N-terminal mitochondrial targeting sequence [49] and co-localizes with mitochondria in various cell types [49, 50]. The Takashi Miyamoto group reported that SARM1 is located on the outer membrane of mitochondria [51, 52]. Evidence from super-resolution microscopy images showing the proximity of SARM1 to the outer mitochondria marker TOM70 (mitochondrial import receptor subunit TOM70) and the inner mitochondria marker ATP5alpha (mitochondrial ATP synthase subunit alpha) forms the basis for this claim. While the data suggest that TOM70 is closer to SARM1 than ATP5alpha, it is challenging to

definitively state that SARM1 is completely separated from ATP5alpha. Therefore, it is difficult to conclusively determine that SARM1 is absent from the inner membrane, even though it may be predominantly present on the outer membrane. Although high-resolution microscopy provides highly accurate data, obtaining observable data at the molecular level presents some challenges.

This study builds upon existing knowledge to provide a more detailed understanding of the molecular-level localization of SARM1. Interestingly, the data from this study not only suggest a high likelihood of SARM1 presence on the inner membrane but also reveal an important finding that interactions between SARM1, cellular stress responses, and actomyosin mediators increase in injured axons. These results indicate that SARM1 can be redistributed within mitochondria using the actomyosin motor within 1 hour of activation. Furthermore, this study also highlights the co-localization of SARM1 with outer mitochondrial membrane proteins such as mitofusin2, TOM70, and TOM22. Particularly noteworthy are the decreased levels of inner mitochondrial membrane proteins in injured axons, with significant reductions observed in mitochondrial import inner membrane translocase subunit TIM23, TIM22, TIM50, and TIM44. This suggests that SARM1 may separate from the inner mitochondrial membrane upon injury. Additionally, the increase in proteins involved in the actomyosin (MYO18A, MYH10, MYH9, etc.) suggests that SARM1 activation may lead to changes in its localization through the actomyosin motor. Additionally, the remodeling of the Actin/Spectrin Membrane-associated Periodic Skeleton (MPS), the collapse of the growth cone resulting in the disintegration of the cytoskeletal structure at the distal end of the axon, and the significant reduction in the amount of F-actin lead to the loss of actin filaments that play a crucial role in maintaining axonal function [53]. The association with SARM1 in this rearrangement has not been previously known; however, this study provides the first hint of this link, thereby expanding the potential functional scope of SARM1 and suggesting new opportunities for its activity. Further study is essential to explore whether the initial activation-induced mitochondrial repositioning of SARM1 and its inhibition of further growth cone elongation, thereby contributing to F-actin redistribution for structural collapse, are involved in axon degeneration induced by injury.

Axon degeneration is a complex process observed in various neurodegenerative diseases and peripheral nerve injuries, making it a significant focus of research in neuroscience. Previous investigations have underscored the pivotal role of the nicotinamide adenine dinucleotide (NAD^+) pathway in both axonal survival and degeneration [8, 37, 54]. NAD^+ acts as a crucial coenzyme in cellular energy metabolism and signaling cascades, playing a particularly vital role in maintaining the stability and functionality of neuronal cells. Depletion of NAD^+ directly influences axonal health, and its insufficiency can trigger the degeneration of axons [55, 56].

Among the three major NAD^+ synthesis pathways, the Salvage Pathway stands out as a primary player in axon degeneration. This pathway functions by recycling nicotinamide to regenerate NAD^+, thereby playing a critical role in sustaining axonal survival and function [57-59]. At the heart of the Salvage Pathway lie two key enzymes: Nicotinamide Phosphoribosyltransferase (NAMPT) and Nicotinamide Mononucleotide Adenylyltransferase (NMNAT). NAMPT, an indispensable enzyme in NAD^+ metabolism, catalyzes the synthesis of the NAD^+ precursor nicotinamide mononucleotide (NMN), which represents a rate-limiting step in NAD^+ biosynthesis. The activity of NAMPT governs intracellular NAD^+ levels, exerting a direct influence on the survival of neuronal cells and the protection of axons [21, 31, 60, 61]. Furthermore, NMNAT, an enzyme responsible for converting NMN into NAD^+, is renowned for its axon-protective properties. The enzymatic activity of NMNAT is crucial for maintaining adequate NAD^+ levels and preventing axonal damage [54, 60, 62-70]. Considering these findings, the modulation of NMNAT and NAMPT activity has emerged as a promising therapeutic strategy for addressing neurodegenerative conditions characterized by axon degeneration.

On the other hand, SARM1 acts as a key protein that promotes Wallerian degeneration, functioning as an auto-inhibited NADase. Upon activation, SARM1 hydrolyzes NAD^+, leading to axon degeneration. Consequently, SARM1 acts as a metabolic sensor regulated by the NMN to NAD^+ ratio [34, 71]. NMN and NAD^+ compete to bind to SARM1's ARM domain, with higher NMN to NAD^+ ratios increasing SARM1 activity and inducing axon degeneration [34]. These two metabolites interact with SARM1, exhibiting opposite effects

upon binding [5, 15, 34, 71-73]. While the physiological ratio of NAD^+ to NMN in axons remains to be determined, studies indicate significantly higher levels of NAD^+ compared to NMN in SGC axons and DRG neurons [36, 37, 47]. Nevertheless, current research has demonstrated therapeutic effects by reducing the NMN to NAD^+ ratio using NAMPT inhibitors [36, 37, 74]. Therefore, the NMN to NAD^+ ratio plays a critical role in regulating axonal damage and degeneration, influencing various physiological and pathological processes related to axonal health.

In this study, I investigated the presence of specific proteins in the vicinity of SARM1 activated by axonal injury, with a particular focus on the key enzymes in the NAD^+ synthesis pathway. As a result of my analysis, while NMNAT was not identified, NAMPT was clearly detected around SARM1. This finding is significant as it suggests that the critical regulatory point in the NAD^+ regeneration pathway, mediated by NAMPT, is maintained even after axonal injury. The presence of NAMPT in damaged axons implies that despite the activation of SARM1, the initial stages of NAD^+ synthesis are still preserved. This indicates that the cells are actively striving to maintain NAD^+ levels following injury, which is crucial for axonal survival and function. Furthermore, I found evidence of a potential interaction between SARM1 and NAMPT, suggesting that SARM1 activation could be promoted through a positive feedback mechanism involving NAMPT. Although the observed increase in the interaction between SARM1 and NAMPT in damaged axons was not statistically significant, it does hint at the possibility of a feedback loop that enhances SARM1 activation. This mechanism could play a pivotal role in the progression of axonal degeneration. In addition, this study explored the therapeutic potential of the novel inhibitor A4276. Effective inhibition of NAMPT by A4276 led to a decrease in the NMN to NAD^+ ratio, which in turn alleviated axonal damage induced by Wallerian degeneration [34]. This finding underscores the importance of maintaining a balanced NMN to NAD^+ ratio in protecting axons from degeneration. Moreover, SARM1 has been identified as a major factor in chemotherapy-induced peripheral neuropathy (CIPN). These experiments demonstrated that low doses of A4276 were effective in mitigating both Wallerian degeneration and CIPN in model systems. This suggests that A4276, when co-administered with chemotherapeutic agents, has the potential to enhance the efficacy of chemotherapy while simultaneously preventing and

alleviating peripheral neuropathy. Modulating this pathway opens up new possibilities for developing novel therapies aimed at preventing axonal degeneration and reducing the side effects of chemotherapy [21].

Further studies should investigate the interaction between SARM1 and NAMPT more thoroughly, particularly examining the relevance of SARM1 activation and its correlation with NAMPT in detail to gain a comprehensive understanding of the underlying mechanisms. This could lead to a deeper exploration and understanding of axon degeneration mechanisms. Additionally, there is a need for research to develop new methods for preventing and treating CIPN, which can have severe side effects. These studies have the potential to contribute to neuroprotection and the treatment of neurological disorders, ultimately improving the quality of life for patients.

I utilized the APEX2 proximity biotinylation system along with LC-MS/MS to identify proteins. Both techniques are highly effective and powerful tools for discovering new proteins or protein-protein interactions. Nevertheless, they also have limitations.

LC-MS/MS (Liquid Chromatography-Tandem Mass Spectrometry) is a widely used analytical technique in modern biology and biochemistry; however, it also has limitations. LC-MS/MS can detect ions at very low concentrations in most cases, but quantifying ions at very low concentrations and within a wide dynamic range can be challenging. While LC-MS/MS can selectively detect specific compounds or ions in most cases, there may be limitations in analyzing specific classes of compounds, especially in complex samples with diverse compounds. Precise detection of specific ions in complex samples with diverse compounds can be challenging. LC-MS/MS analysis often requires complex sample pretreatment processes, which can lead to sample loss. Interpreting LC-MS/MS data can be complex and challenging, especially processing and understanding large amounts of data. The analysis can be relatively slow, and it requires significant time, cost, equipment, and expertise to analyze large samples. Obtaining accurate results can be difficult due to various issues during the analysis process, including sample contamination, ionization difficulties, noise, and background signals. These limitations need to be considered depending on the

field of application and sample characteristics, and research and new methodologies and techniques need to be developed to overcome these limitations.

The APEX2 proximity biotinylation system is a powerful tool; however, it has several limitations. Firstly, it relies on labeling the proximity of specific proteins, which does not guarantee specific interactions with the desired protein and can lead to non-specific labeling, complicating data interpretation and challenging the system's specificity. Secondly, it may have limitations in detecting low-level protein interactions, particularly with low abundance or weak interactions. Thirdly, the system's resolution is often limited, making it challenging to accurately detect small structures or short interactions. Fourthly, changes in protein localization or activity due to specific conditions or stimuli within the cell can affect the proximity biotinylation results, and detecting interactions of inactive or deficient proteins may also be difficult. Lastly, interpreting and utilizing the results of the APEX2 system requires consideration of these limitations. Conducting numerous replicates and experiments under the same conditions, along with additional experimental approaches and data analysis techniques, are necessary to overcome these constraints.

To overcome the limitations of these techniques, this study conducted LC-MS/MS analysis on 4 biological replicate samples. To create a consistent experimental environment, a single clone of cells was cultured and subjected to affinity purification on the same day. Recently, there has been an attempt to investigate protein changes in SARM1-dependent axon degeneration research using the APEX2 proximity biotinylation system by a particular group. In their study, they examined the interactome of SARM1 to understand its function and identify new molecules [75]. Through this process, they found that overexpression of USP13 delayed axon degeneration induced by injury, highlighting its crucial role in promoting self-inhibition of SARM1. These findings suggest that increasing USP13 activity may offer a strategy to alleviate axon degeneration. However, a limitation of this group's approach is that they investigated the interactome by identifying proteins interacting with each domain of inactive SARM1. Therefore, it can be inferred that identifying proteins interacting directly with both inactive and active SARM1 in the early axonal destruction program from direct axonal injury could be of great significance.

Thus, this study will contribute to the discovery of the mechanism of SARM1 activation in axon degeneration and help design new strategies to prevent neurodegeneration associated with injury or disease.

5. Conclusion

1. SH-SY5Y neuronal cell line with SARM1-APEX2 was generated.
2. SARM1-APEX2 is functional and mediates Wallerian degeneration.
3. Proximity biotinylation of SARM1-APEX2 in axons was performed with or without axotomy, marking the first instance of such experimentation.
4. Affinity purification and mass spectrometry analysis indicated SARM1 dissociation from mitochondria upon activation and identified proteins selectively binding to inactive or active SARM1.
5. Functional validation of a facilitator of axon degeneration (NAMPT) was performed.

References

1. Waller, A., Experiments on the Section of the Glosso-Pharyngeal and Hypoglossal Nerves of the Frog, and Observations of the Alterations Produced Thereby in the Structure of Their Primitive Fibres. Edinb Med Surg J, 1851. **76**(189): p. 369-376.

2. Coleman, M.P. and A. Hoke, *Programmed axon degeneration: from mouse to mechanism to medicine.* Nat Rev Neurosci, 2020. **21**(4): p. 183-196.

3. Figley, M.D. and A. DiAntonio, *The SARM1 axon degeneration pathway: control of the NAD(+) metabolome regulates axon survival in health and disease.* Curr Opin Neurobiol, 2020. **63**: p. 59-66.

4. Neukomm, L.J. and M.R. Freeman, *Diverse cellular and molecular modes of axon degeneration.* Trends Cell Biol, 2014. **24**(9): p. 515-23.

5. Jiang, Y., T. Liu, C.H. Lee, Q. Chang, J. Yang, and Z. Zhang, *The NAD(+)-mediated self-inhibition mechanism of pro-neurodegenerative SARM1.* Nature, 2020. **588**(7839): p. 658-663.

6. Osterloh, J.M., J. Yang, T.M. Rooney, A.N. Fox, R. Adalbert, E.H. Powell, et al., *dSarm/Sarm1 is required for activation of an injury-induced axon death pathway.* Science, 2012. **337**(6093): p. 481-4.

7. Neukomm, L.J., T.C. Burdett, A.M. Seeds, S. Hampel, J.C. Coutinho-Budd, J.E. Farley, et al., *Axon Death Pathways Converge on Axundead to Promote Functional and Structural Axon Disassembly.* Neuron, 2017. **95**(1): p. 78-91 e5.

8. Gerdts, J., E.J. Brace, Y. Sasaki, A. DiAntonio, and J. Milbrandt, *SARM1 activation triggers axon degeneration locally via NAD(+) destruction.* Science, 2015. **348**(6233): p. 453-7.

9. Essuman, K., D.W. Summers, Y. Sasaki, X. Mao, A. DiAntonio, and J. Milbrandt, *The SARM1 Toll/Interleukin-1 Receptor Domain Possesses Intrinsic NAD(+) Cleavage Activity that*

Promotes Pathological Axonal Degeneration. Neuron, 2017. **93**(6): p. 1334-1343 e5.

10. Gerdts, J., D.W. Summers, Y. Sasaki, A. DiAntonio, and J. Milbrandt, *Sarm1-mediated axon degeneration requires both SAM and TIR interactions.* J Neurosci, 2013. **33**(33): p. 13569-80.

11. Horsefield, S., H. Burdett, X. Zhang, M.K. Manik, Y. Shi, J. Chen, et al., *NAD(+) cleavage activity by animal and plant TIR domains in cell death pathways.* Science, 2019. **365**(6455): p. 793-799.

12. Hung, V., N.D. Udeshi, S.S. Lam, K.H. Loh, K.J. Cox, K. Pedram, et al., *Spatially resolved proteomic mapping in living cells with the engineered peroxidase APEX2.* Nat Protoc, 2016. **11**(3): p. 456-75.

13. Martell, J.D., T.J. Deerinck, Y. Sancak, T.L. Poulos, V.K. Mootha, G.E. Sosinsky, et al., *Engineered ascorbate peroxidase as a genetically encoded reporter for electron microscopy.* Nat Biotechnol, 2012. **30**(11): p. 1143-8.

14. Lobingier, B.T., R. Huttenhain, K. Eichel, K.B. Miller, A.Y. Ting, M. von Zastrow, and N.J. Krogan, *An Approach to Spatiotemporally Resolve Protein Interaction Networks in Living Cells.* Cell, 2017. **169**(2): p. 350-360 e12.

15. Zhao, Z.Y., X.J. Xie, W.H. Li, J. Liu, Z. Chen, B. Zhang, et al., *A Cell-Permeant Mimetic of NMN Activates SARM1 to Produce Cyclic ADP-Ribose and Induce Non-apoptotic Cell Death.* iScience, 2019. **15**: p. 452-466.

16. Kovalevich, J., M. Santerre, and D. Langford, *Considerations for the Use of SH-SY5Y Neuroblastoma Cells in Neurobiology.* Methods Mol Biol, 2021. **2311**: p. 9-23.

17. Shipley, M.M., C.A. Mangold, and M.L. Szpara, *Differentiation of the SH-SY5Y Human Neuroblastoma Cell Line.* J Vis Exp, 2016(108): p. 53193.

18. Rhee, H.W., P. Zou, N.D. Udeshi, J.D. Martell, V.K. Mootha, S.A. Carr, and A.Y. Ting, *Proteomic mapping of mitochondria in living cells via spatially restricted enzymatic tagging.*

Science, 2013. **339**(6125): p. 1328-1331.

19. Remy, O. and Y.G. Santin, *Identification of Protein Partners by APEX2 Proximity Labeling.* Methods Mol Biol, 2024. **2715**: p. 321-329.

20. Choi, B., H. Kim, J. Jang, S. Park, and H. Jung, *Development and Degeneration of Retinal Ganglion Cell Axons in Xenopus tropicalis.* Mol Cells, 2022. **45**(11): p. 846-854.

21. Kim, M., H. Kim, B.G. Kang, J. Lee, T. Kim, H. Lee, et al., *Discovery of a novel NAMPT inhibitor that selectively targets NAPRT-deficient EMT-subtype cancer cells and alleviates chemotherapy-induced peripheral neuropathy.* Theranostics, 2023. **13**(14): p. 5075-5098.

22. Yeo, S., J. Jang, H.J. Jung, H. Lee, and Y. Choe, *Primary cilia-mediated regulation of microglial secretion in Alzheimer's disease.* Front Mol Biosci, 2023. **10**: p. 1250335.

23. Shin, J.E. and Y. Cho, *Assessing Axonal Degeneration in Embryonic Dorsal Root Ganglion Neurons In Vitro.* Methods Mol Biol, 2020. **2143**: p. 41-54.

24. Ran, F.A., P.D. Hsu, J. Wright, V. Agarwala, D.A. Scott, and F. Zhang, *Genome engineering using the CRISPR-Cas9 system.* Nat Protoc, 2013. **8**(11): p. 2281-2308.

25. Yong, Y., K. Gamage, C. Cushman, A. Spano, and C. Deppmann, *Regulation of degenerative spheroids after injury.* Sci Rep, 2020. **10**(1): p. 15472.

26. Yang, J., Z. Wu, N. Renier, D.J. Simon, K. Uryu, D.S. Park, et al., *Pathological axonal death through a MAPK cascade that triggers a local energy deficit.* Cell, 2015. **160**(1-2): p. 161-76.

27. Shin, J.E., Y. Cho, B. Beirowski, J. Milbrandt, V. Cavalli, and A. DiAntonio, *Dual leucine zipper kinase is required for retrograde injury signaling and axonal regeneration.* Neuron, 2012. **74**(6): p. 1015-22.

28. Shin, J.E., B.R. Miller, E. Babetto, Y. Cho, Y. Sasaki, S. Qayum, et al., *SCG10 is a JNK target in the axonal degeneration pathway.* Proc Natl Acad Sci U S A, 2012. **109**(52): p. E3696-705.

29. Subramanian, A., P. Tamayo, V.K. Mootha, S. Mukherjee, B.L. Ebert, M.A. Gillette, et al., *Gene set enrichment analysis: a knowledge-based approach for interpreting genome-wide expression profiles.* Proc Natl Acad Sci U S A, 2005. **102**(43): p. 15545-50.

30. Wang, P., Y. Lu, D. Han, P. Wang, L. Ren, J. Bi, and J. Liang, *Neuroprotection by nicotinamide mononucleotide adenylyltransferase 1 with involvement of autophagy in an aged rat model of transient cerebral ischemia and reperfusion.* Brain Res, 2019. **1723**: p. 146391.

31. Yao, Z., W. Yang, Z. Gao, and P. Jia, *Nicotinamide mononucleotide inhibits JNK activation to reverse Alzheimer disease.* Neurosci Lett, 2017. **647**: p. 133-140.

32. Wang, X., X. Hu, Y. Yang, T. Takata, and T. Sakurai, *Nicotinamide mononucleotide protects against beta-amyloid oligomer-induced cognitive impairment and neuronal death.* Brain Res, 2016. **1643**: p. 1-9.

33. Loreto, A., M. Di Stefano, M. Gering, and L. Conforti, *Wallerian Degeneration Is Executed by an NMN-SARM1-Dependent Late Ca(2+) Influx but Only Modestly Influenced by Mitochondria.* Cell Rep, 2015. **13**(11): p. 2539-2552.

34. Figley, M.D., W. Gu, J.D. Nanson, Y. Shi, Y. Sasaki, K. Cunnea, et al., *SARM1 is a metabolic sensor activated by an increased NMN/NAD(+) ratio to trigger axon degeneration.* Neuron, 2021.

35. Shi, Y., P.S. Kerry, J.D. Nanson, T. Bosanac, Y. Sasaki, R. Krauss, et al., *Structural basis of SARM1 activation, substrate recognition, and inhibition by small molecules.* Mol Cell, 2022. **82**(9): p. 1643-1659 e10.

36. Liu, H.W., C.B. Smith, M.S. Schmidt, X.A. Cambronne, M.S. Cohen, M.E. Migaud, et al., *Pharmacological bypass of NAD(+) salvage pathway protects neurons from chemotherapy-induced degeneration.* Proc Natl Acad Sci U S A, 2018. **115**(42): p. 10654-10659.

37. Di Stefano, M., I. Nascimento-Ferreira, G. Orsomando, V. Mori, J. Gilley, R. Brown, et al., *A rise in NAD precursor nicotinamide mononucleotide (NMN) after injury promotes axon degeneration.* Cell Death Differ, 2015. **22**(5): p. 731-42.

38. Alano, C.C., P. Garnier, W. Ying, Y. Higashi, T.M. Kauppinen, and R.A. Swanson, *NAD+ depletion is necessary and sufficient for poly(ADP-ribose) polymerase-1-mediated neuronal death.* J Neurosci, 2010. **30**(8): p. 2967-78.

39. Hasmann, M. and I. Schemainda, *FK866, a highly specific noncompetitive inhibitor of nicotinamide phosphoribosyltransferase, represents a novel mechanism for induction of tumor cell apoptosis.* Cancer Res, 2003. **63**(21): p. 7436-42.

40. Court, F.A. and M.P. Coleman, *Mitochondria as a central sensor for axonal degenerative stimuli.* Trends Neurosci, 2012. **35**(6): p. 364-72.

41. Wang, B., M. Huang, D. Shang, X. Yan, B. Zhao, and X. Zhang, *Mitochondrial Behavior in Axon Degeneration and Regeneration.* Front Aging Neurosci, 2021. **13**: p. 650038.

42. Merlini, E., M.P. Coleman, and A. Loreto, *Mitochondrial dysfunction as a trigger of programmed axon death.* Trends Neurosci, 2022. **45**(1): p. 53-63.

43. Campbell, G. and D.J. Mahad, *Mitochondrial dysfunction and axon degeneration in progressive multiple sclerosis.* FEBS Lett, 2018. **592**(7): p. 1113-1121.

44. Devine, M.J. and J.T. Kittler, *Mitochondria at the neuronal presynapse in health and disease.* Nat Rev Neurosci, 2018. **19**(2): p. 63-80.

45. Klemmensen, M.M., S.H. Borrowman, C. Pearce, B. Pyles, and B. Chandra, *Mitochondrial dysfunction in neurodegenerative disorders.* Neurotherapeutics, 2024. **21**(1): p. e00292.

46. Kitay, B.M., R. McCormack, Y. Wang, P. Tsoulfas, and R.G. Zhai, *Mislocalization of neuronal mitochondria reveals regulation of Wallerian degeneration and NMNAT/WLD(S)-mediated axon protection independent of axonal mitochondria.* Hum Mol Genet, 2013. **22**(8): p. 1601-14.

47. Sasaki, Y., T.M. Engber, R.O. Hughes, M.D. Figley, T. Wu, T. Bosanac, et al., *cADPR is a gene dosage-sensitive biomarker of SARM1 activity in healthy, compromised, and degenerating axons.* Exp Neurol, 2020. **329**: p. 113252.

48. Summers, D.W., A. DiAntonio, and J. Milbrandt, *Mitochondrial dysfunction induces Sarm1-dependent cell death in sensory neurons.* J Neurosci, 2014. **34**(28): p. 9338-50.

49. Panneerselvam, P., L.P. Singh, B. Ho, J. Chen, and J.L. Ding, *Targeting of pro-apoptotic TLR adaptor SARM to mitochondria: definition of the critical region and residues in the signal sequence.* Biochem J, 2012. **442**(2): p. 263-71.

50. Kim, Y., P. Zhou, L. Qian, J.Z. Chuang, J. Lee, C. Li, et al., *MyD88-5 links mitochondria, microtubules, and JNK3 in neurons and regulates neuronal survival.* J Exp Med, 2007. **204**(9): p. 2063-74.

51. Miyamoto T, C.K., Johann Chow, J. Dugas, Jack D. DeGroot, A. Bagdasarian, Arun P. Thottumkara, M. Larhammar, M. Calvert, B. Fox, Joseph W. Lewcock, L. A. Kane *SARM1 activation and its downstreampathways are distinct in neuronal compartments.* bioRxiv, 2019. **2019;9–25**.

52. Miyamoto, T., C. Kim, J. Chow, J.C. Dugas, J. DeGroot, A.L. Bagdasarian, et al., *SARM1 is responsible for calpain-dependent dendrite degeneration in mouse hippocampal neurons.* J Biol Chem, 2024. **300**(2): p. 105630.

53. Unsain, N., M.D. Bordenave, G.F. Martinez, S. Jalil, C. von Bilderling, F.M. Barabas, et al., *Remodeling of the Actin/Spectrin Membrane-associated Periodic Skeleton, Growth Cone Collapse and F-Actin Decrease during Axonal Degeneration.* Sci Rep, 2018. **8**(1): p. 3007.

54. Araki, T., Y. Sasaki, and J. Milbrandt, *Increased nuclear NAD biosynthesis and SIRT1 activation prevent axonal degeneration.* Science, 2004. **305**(5686): p. 1010-3.

55. Hou, Y., Y. Wei, S. Lautrup, B. Yang, Y. Wang, S. Cordonnier, et al., *NAD(+) supplementation reduces neuroinflammation and cell senescence in a transgenic mouse model of Alzheimer's disease via cGAS-STING.* Proc Natl Acad Sci U S A, 2021. **118**(37).

56. Wang, X., H.J. He, X. Xiong, S. Zhou, W.W. Wang, L. Feng, et al., *NAD(+) in Alzheimer's Disease: Molecular Mechanisms and Systematic Therapeutic Evidence Obtained in vivo.* Front Cell Dev Biol, 2021. **9**: p. 668491.

57. Katsyuba, E., M. Romani, D. Hofer, and J. Auwerx, *NAD(+) homeostasis in health and disease.* Nat Metab, 2020. **2**(1): p. 9-31.

58. Xie, N., L. Zhang, W. Gao, C. Huang, P.E. Huber, X. Zhou, et al., *NAD(+) metabolism: pathophysiologic mechanisms and therapeutic potential.* Signal Transduct Target Ther, 2020. **5**(1): p. 227.

59. Canto, C., K.J. Menzies, and J. Auwerx, *NAD(+) Metabolism and the Control of Energy Homeostasis: A Balancing Act between Mitochondria and the Nucleus.* Cell Metab, 2015. **22**(1): p. 31-53.

60. Gilley, J., G. Orsomando, I. Nascimento-Ferreira, and M.P. Coleman, *Absence of SARM1 rescues development and survival of NMNAT2-deficient axons.* Cell Rep, 2015. **10**(12): p. 1974-81.

61. Sasaki, Y., B.P. Vohra, F.E. Lund, and J. Milbrandt, *Nicotinamide mononucleotide adenylyl transferase-mediated axonal protection requires enzymatic activity but not increased levels of neuronal nicotinamide adenine dinucleotide.* J Neurosci, 2009. **29**(17): p. 5525-35.

62. Di Stefano, M., A. Loreto, G. Orsomando, V. Mori, F. Zamporlini, R.P. Hulse, et al., *NMN Deamidase Delays Wallerian Degeneration and Rescues Axonal Defects Caused by NMNAT2 Deficiency In Vivo.* Curr Biol, 2017. **27**(6): p. 784-794.

63. Gilley, J., R. Adalbert, G. Yu, and M.P. Coleman, *Rescue of peripheral and CNS axon defects in mice lacking NMNAT2.* J Neurosci, 2013. **33**(33): p. 13410-24.

64. Gilley, J. and M.P. Coleman, *Endogenous Nmnat2 is an essential survival factor for maintenance of healthy axons.* PLoS Biol, 2010. **8**(1): p. e1000300.

65. Gilley, J., P.R. Mayer, G. Yu, and M.P. Coleman, *Low levels of NMNAT2 compromise axon development and survival.* Hum Mol Genet, 2019. **28**(3): p. 448-458.

66. Huppke, P., E. Wegener, J. Gilley, C. Angeletti, I. Kurth, J.P.H. Drenth, et al., *Homozygous NMNAT2 mutation in sisters with polyneuropathy and erythromelalgia.* Exp Neurol, 2019.

320: p. 112958.

67. Milde, S., J. Gilley, and M.P. Coleman, *Axonal trafficking of NMNAT2 and its roles in axon growth and survival in vivo.* Bioarchitecture, 2013. **3**(5): p. 133-40.

68. Sasaki, Y., T. Nakagawa, X. Mao, A. DiAntonio, and J. Milbrandt, *NMNAT1 inhibits axon degeneration via blockade of SARM1-mediated NAD(+) depletion.* Elife, 2016. **5**.

69. Tarasiuk, O., L. Molteni, A. Malacrida, and G. Nicolini, *The Role of NMNAT2/SARM1 in Neuropathy Development.* Biology (Basel), 2024. **13**(1).

70. Yang, S., Z.X. Niou, A. Enriquez, J. LaMar, J.Y. Huang, K. Ling, et al., *NMNAT2 supports vesicular glycolysis via NAD homeostasis to fuel fast axonal transport.* Mol Neurodegener, 2024. **19**(1): p. 13.

71. Bratkowski, M., T. Xie, D.A. Thayer, S. Lad, P. Mathur, Y.S. Yang, et al., *Structural and Mechanistic Regulation of the Pro-degenerative NAD Hydrolase SARM1.* Cell Rep, 2020. **32**(5): p. 107999.

72. Angeletti, C., A. Amici, J. Gilley, A. Loreto, A.G. Trapanotto, C. Antoniou, et al., *SARM1 is a multi-functional NAD(P)ase with prominent base exchange activity, all regulated bymultiple physiologically relevant NAD metabolites.* iScience, 2022. **25**(2): p. 103812.

73. Sporny, M., J. Guez-Haddad, T. Khazma, A. Yaron, M. Dessau, Y. Shkolnisky, et al., *Structural basis for SARM1 inhibition and activation under energetic stress.* Elife, 2020. **9**.

74. Bosanac, T., R.O. Hughes, T. Engber, R. Devraj, A. Brearley, K. Danker, et al., *Pharmacological SARM1 inhibition protects axon structure and function in paclitaxel-induced peripheral neuropathy.* Brain, 2021. **144**(10): p. 3226-3238.

75. Yue, W., K. Zhang, M. Jiang, W. Long, J. Cui, Y. Li, et al., *Deubiquitination of SARM1 by USP13 regulates SARM1 activation and axon degeneration.* Life Medicine, 2023. **2**(5).

Abstract in Korean

SARM1 의존적 축삭 파괴 프로그램 기전 규명

1850년에 August Waller는 세포체에서 분리된 말단 축삭 조각의 전형적인 분해를 기술하였으며, 이를 월러변성 (Wallerian degeneration)이라고 합니다. 최근에서야 월러변성 과 질병과 관련된 비분리된 축삭의 변성, 특히 죽어 가는 후퇴성 축삭 변성이 분자 기작과 실행자를 공유한다는 것이 확립되었습니다. 주요 분자 중 하나는 SARM1입니다. *SARM1* 유전자의 유전자 삭제는 월러변성을 예방하며, 따라서 현재의 노력은 화학 요법 유발 말단 축삭 변성 (예: 화학 요법 유발 말단 신경병증) 및 질병 관련 후퇴성 축삭 변성 (예: 파킨슨병 및 경도 전층 경화증)과 같은 손상 유발 말단 축삭 변성에서 그 억제가 치료적인지에 중점을 두고 있습니다. 처음에는 Toll 유사 수용체 어댑터 단백질로서 기술되었지만, 최근에는 *SARM1*의 TIR 도메인이 예상치 못한 니코틴아마이드 아데닌 디뉴클레오타이드 (NAD^+) 가수분해 효소 (NADase) 활동을 가지고 있음이 밝혀졌습니다. 이는 이성질화에 의해 활성화되며, NAD^+를 니코틴아마이드와 아데닌 이인산 리보스 (ADP-리보스 또는 ADPR) 또는 사이클릭 ADPR (cADPR)로 가수분해하는 반응을 촉매화합니다. 이로써, SARM1은 치료 대상이 될 수 있습니다. SARM1 NADase 활동의 소분자 억제제 개발은 활발한 연구 분야입니다. 축삭 변성에 대한 명확한 역할에도 불구하고, SARM1은 건강한 축삭에서도 발견되며, 상처나 질병 발생 후에만 그 NADase 활동이 활성화되는 방법은 알려져 있지 않습니다. 저의 논문의 전반적인 목표는 정상적인 및 질병에 걸린 축삭에서 SARM1의 자가억제 및 활성화에 관여하는 단백질 후보군을 식별하고 관련된 분자 기작을 제시하는 것입니다. 이를 위해, 저는 APEX2 proximity biotinylation assay를 통해 활성화 또는 비활성화 상태에 특이적인 SARM1 상호 작용체를 분리 동정했습니다. 정상 축삭과 손상된 축삭에서 affinity purification을 하고 대량질량분석을 통해 대략 1000개의 SARM1 의존적 축삭 파괴프로그램에 관련된 단백질을 성공적으로 식별했습니다. SARM1의 활성화 및

비활성화 시 축삭에서의 상호작용체를 통해 총 2가지의 결론을 도출할 수 있었습니다. 첫째, 부상에 대한 반응으로 SARM1 단백질의 세포 내 위치가 변화하는 증거를 발견했습니다. Gene Set Enrichment Analysis (GSEA)에 따르면 SARM1과 미토콘드리아 단백질 간의 상호 작용이 감소합니다. 이와는 대조적으로, cellular stress responses 와 actomyosin 간의 상호 작용은 손상된 축삭에서 증가합니다. 이러한 결과는 비활성 SARM1 단백질이 미토콘드리아에 도킹되어 있을 수 있고 actomyosin motor를 사용하여 다른 곳으로 이동시킬 수 있다는 것입니다. 둘째, SARM1과 니코티나마이드 포스포리보실트랜스페라아제(NAMPT) 간의 상호 작용이 SARM1 활성화를 촉진할 수 있다는 증거를 발견했습니다. NAMPT는 니코틴아마이드를 니코티나미드 모노뉴클레오티드(NMN)로 변환하며, 이는 SARM1 활성을 증가시키는 것으로 알려져 있습니다. 부상을 입은 축삭에서 SARM1과 NAMPT 간 상호 작용이 약간 증가한 것을 발견했는데, 이는 SARM1 활성화에 긍정적인 반응 메커니즘을 시사합니다. 이 결과와 일치하게, NAMPT의 새롭게 개발된 소분자 억제제는 월러변성 및 화학 요법 유발 말단 신경병증을 지연시켰습니다. 요약하자면, 축삭 손상에 대한 반응으로 SARM1 단백질과 관련된 단백질을 식별하고 의도된 대로 그들의 상호 작용이 변하는 두 개의 새로운 발견을 하였으며, 이는 SARM1 활성화 및 그 예방을 이해하기 위한 분자 기전에 관련된 깊은 이해에 기여할 것으로 예상됩니다. 이 학위 논문에서의 새로운 데이터셋과 결과는 질병과 손상을 입은 축삭에서의 SARM1 활성화에 대한 깊은 이해에 기여할 뿐만 아니라 SARM1 활성화 및 SARM1−의존적 축삭 변성 및 신경퇴행성 질환을 예방하기 위한 치료 전략에 대한 통찰을 제공할 수 있습니다.

핵심되는 말: SARM1, 축삭 파괴, 월러 변성, 신경병증

Publication list

1. *Kim M, ***Kim H**, Kang BG, Lee J, Kim T, Lee H et al (2023) Discovery of a novel NAMPT inhibitor that selectively targets NAPRT-deficient EMT-subtype cancer cells and alleviates chemotherapy-induced peripheral neuropathy ***Theranostics*** 13(14):5075-5098 (*equal contributors, †corresponding authors).

2. *Jung J, *Ohk J, ***Kim H**, Holt CE, †Park HJ, †Jung H (2023) mRNA transport, translation, and decay in adult mammalian central nervous system axons. ***Neuron*** 111: 650-668 (*equal contributors, †corresponding authors).

3. *Choi B, ***Kim H**, Jang J, Park S, †Jung H (2022) Development and Degeneration of Retinal Ganglion Cell Axons in *Xenopus tropicalis* (Cover image) ***Mol Cells*** 45(11):846-854 (*equal contributors, †corresponding author).

4. Lee H, Chin H, **Kim H**, Jung H, Lee D. STAT3-mediated MLST8 gene expression regulates cap-dependent translation in cancer cells. ***Mol Oncol*** 2020;14: 1850–1867